EUROPEAN ORGANIZATION FOR NUCLEAR RESEARCH

CERN-EP/85- 166
October 9th, 1985

MEASUREMENT OF $W^{\pm}$ AND Z^0 PROPERTIES AT THE CERN $\bar{p}p$ COLLIDER

The UA2 Collaboration

Bern[1] - CERN[2] - Copenhagen (NBI)[3] - Heidelberg[4] - Orsay (LAL)[5] - Pavia[6] - Perugia[7] - Pisa[8] - Saclay (CEN)[9] Collaboration

J.A. Appel[9,a], P. Bagnaia[2], M. Banner[9], R. Battiston[7], K. Bernlöhr[4], K. Borer[1], M. Borghini[2], G. Carboni[8], V. Cavasinni[8], P. Cenci[7,b], J.-C. Chollet[5], A.G. Clark[2], A. Codino[7], C. Conta[6], P. Darriulat[2], B. De Lotto[5], T. Del Prete[8], L. Di Lella[2], J. Dines-Hansen[3], K. Einsweiler[2], R. Engelmann[2,c], L. Fayard[5], M. Fraternali[6], D. Froidevaux[5], J.-M. Gaillard[5], O. Gildemeister[2], V.G. Goggi[6], C. Gössling[2], B. Hahn[1], H. Hänni[1], J.R. Hansen[2], P. Hansen[2,3], N. Harnew[2], T. Himel[2,d], L. Iconomidou-Fayard[5], K. Jakobs[4], P. Jenni[2], E.E. Kluge[4], O. Kofoed-Hansen[3], E. Lançon[9], M. Livan[6], S. Loucatos[9], B. Madsen[3], P. Mani[1], B. Mansoulié[9], G.C. Mantovani[7], L. Mapelli[2,e], K. Meier[2], B. Merkel[5], R. Mollerud[3], M. Moniez[5], R. Moning[1], M. Morganti[8], B. Nilsson[3], C. Onions[2], M.A. Parker[2], G. Parrour[5], F. Pastore[6], M. Pepe[7], H. Plothow-Besch[4], M. Polverel[9], A. Putzer[4], J.-P. Repellin[5], A.F. Rothenberg[2,d], A. Roussarie[9], V. Ruhlmann[9], G. Sauvage[5], J. Schacher[1], M. Schlötelburg[4], F. Stocker[1], M. Swartz[2], J. Teiger[9], K. Tittel[4], S.N. Tovey[2,f], W.Y. Tsang[g], M. Valdata-Nappi[8], V. Vercesi[6], A.R. Weidberg[2], M. Wunsch[4] and H. Zaccone[9].

ABSTRACT

A study of $W^{\pm}$ and Z^0 properties has been performed using the UA2 detector at the CERN $\bar{p}p$ collider. The data correspond to a total integrated luminosity of $142\,nb^{-1}$ at $\sqrt{s} = 546$ GeV, and of $310\,nb^{-1}$ at $\sqrt{s} = 630$ GeV. The experimental results are compared to the predictions of the Standard Model of the unified electroweak theory.

(Submitted to Zeitschrift für Physik C - Particles and Fields)

---

1. Laboratorium für Hochenergiephysik, Universität Bern, Sidlerstrasse 5, Bern, Switzerland.

2. CERN, 1211 Geneva 23, Switzerland.

3. Niels Bohr Institute, Blegdamsvej 17, Copenhagen, Denmark.

4. Institut für Hochergiephysik der Universität Heidelberg, Schröderstrasse 90, 6900 Heidelberg, FRG.

5. Laboratoire de l'Accélérateur Linéaire, Université de Paris-Sud, Orsay, France.

6. Dipartimento di Fisica Nucleare e Teorica, Università di Pavia and INFN, Sezione di Pavia, Via Bassi 6, Pavia, Italy.

7. Gruppo INFN del Dipartimento di Fisica dell'Università di Perugia, Italy.

8. Dipartimento di fisica dell'Università di Pisa and INFN, Sezione di Pisa, Via Livornese, S. Piero a Grado, Pisa, Italy.

9. Centre d'Etudes Nucléaires de Saclay, France.

a) On leave from FNAL, Batavia, Illinois, USA.

b) Also at Scuola Normale Superiore, Pisa, Italy.

c) On leave from New York State University, Stony Brook, NY, USA.

d) Now at SLAC, Stanford University, Stanford, California, USA.

e) On leave from INFN, Pavia, Italy.

f) Visitor from the University of Melbourne, Victoria, Australia.

g) Cavendish Laboratory, University of Cambridge, Cambridge, U.K.

1. INTRODUCTION

In previous publications [1-3] we reported experimental results on the processes

$$\bar{p} + p \rightarrow W^{\pm} + \text{anything}$$
$$\rightarrow e^{\pm} + \nu(\bar{\nu}) + \text{anything}$$

and

$$\bar{p} + p \rightarrow Z^0 + \text{anything}$$
$$\rightarrow e^+ + e^- + \text{anything}$$

where $W^{\pm}$ and Z^0 are the Intermediate Vector Bosons (IVB) of the unified electroweak theory. The data were collected at the CERN $\bar{p}p$ Collider in the period between October 1982 and June 1983 at a total centre-of-mass energy $\sqrt{s} = 546$ GeV. The total integrated luminosity accumulated by the UA2 experiment during that period was $L = 142\ nb^{-1}$.

In the subsequent data-taking run during the Autumn of 1984 the collider provided $\bar{p}p$ collisions at an increased $\sqrt{s}$ value, $\sqrt{s} = 630$ GeV, and the total integrated luminosity accumulated by the UA2 experiment was $L = 310\ nb^{-1}$.

We report here the final results from a study of $W^{\pm}$ and Z^0 properties using the whole data sample ($L = 452\ nb^{-1}$). Because of the more than three-fold increase in luminosity with respect to the data sample previously available [3], we obtain a higher statistical precision in the determination of the IVB masses, $W^{\pm}$ decay asymmetry and Z^0 width.

We also study the $W^{\pm}$ and Z^0 production properties. In particular, we compare the cross-sections measured at the two available $\sqrt{s}$ values. In addition, we study the associated production of IVB's and high-p_T hadronic jets and we compare these observations with the expectations from higher-order QCD corrections to the basic production subprocesses.

Finally, we compare the measured masses and widths of the $W^{\pm}$ and Z^0 with predictions of the Standard Model. No significant deviations from the Standard Model predictions are observed.

2. CALORIMETER ENERGY MEASUREMENT

The UA2 detector has been described elsewhere [3,4]. Since the precision of the $W^{\pm}$ and Z^0 mass determination is dependent on the accurate measurement of electron energies, and the data have been collected over a period of two years, the stability of the calorimeters used for these measurements plays a crucial role.

All calorimeter cells (480 in total) were initially calibrated in 1981 using 10 GeV electron and muon beams from the CERN PS. At that time, the calibration was uniform in E_T to within $\sim \pm 0.5\%$ from cell-to-cell. The calibration stability has since been monitored by means of three independent methods :

i. each calorimeter module is equipped with a light-flasher system, which includes a light stability monitor. The system is used to correct the variations of the calibration constants that occur over the relatively short duration of a Collider run (typically three to four months). In addition, a single stability monitor tracks the inter-module calibration of the 24 modules of the central calorimeter [5].

ii. before and after each run, a movable Co^{60} radioactive source is precisely located in front of each calorimeter cell and the direct current induced in the photomultipliers is then measured. This method is used to monitor the long-term stability of the front section of the calorimeter.

iii. a direct measurement of the calibration stability for each module of the central calorimeter [5] is also obtained from the average energy flow observed in unbiased $\bar{p}p$ collisions.

These three methods provide a way to correct for the drift of the calorimeter response as a function of time. The effectiveness of this correction was checked by recalibrating eight modules of the central calorimeter using a beam from the PS in December 1982. Two additional modules were checked using a beam from the SPS a year later.

We observe a decrease of the overall calorimeter response to particles of a given energy. The average drift in the electromagnetic calorimeters amounts to $\sim -6\%$ per year when no Collider run takes place. There is an additional deterioration of the response during Collider runs as a result of radiation damage to the scintillator and light-collection system. For a typical three-month run the resulting additional drift amounts to $\sim -3\%$.

These rather large drifts are almost completely taken into account by the calibration-stability monitors described above. After a period of approximately 4 years since the original calibration, the present uncertainty on the absolute energy scale of the electromagnetic calorimeters amounts to $\pm$ 1.5%, with a cell-to-cell variation of zero mean and 2.5% r.m.s. spread. The corresponding values for the first compartment of the hadronic calorimeter are respectively $\pm$ 6.5% and 8%, mainly because the method based on the use of the Co^{60} source cannot be applied to this part of the detector. The effect of these latter uncertainties on the measurement of the electron energies is negligible because the energy leakage of electromagnetic showers into the hadronic calorimeter is generally not more than 10%.

An additional systematic uncertainty on the absolute energy scale arises from the time-variation of the light-attenuation properties of the scintillators. This enters into the correction of the measured particle energies as a function of the impact point on the calorimeter, and is estimated to be $\pm$ 0.3% on average.

The total systematic uncertainty on the measured electron energy deposition in the calorimeter is estimated to be $\pm$ 1.6% on average.

3. DATA TAKING AND ANALYSIS

As for the 1982-83 Collider runs, two triggers were used to select events containing $W^{\pm} \rightarrow e^{\pm}\nu(\bar{\nu})$ or $Z^0 \rightarrow e^+e^-$ decays :

i. the W-trigger, which required a cluster of transverse energy deposition $E_T > 10$ GeV in any matrix of 2 × 2 adjacent cells of the electromagnetic calorimeter. For the central calorimeter, all possible 2 × 2 matrices were considered. For the two forward calorimeters, only those 2 × 2 matrices corresponding to a given calorimeter module (24 modules in all) were considered.

ii. the Z^0-trigger, which required the simultaneous presence of two such clusters above a threshold $E_T > 4.5$ GeV, separated in azimuth by at least 60°.

The total number of W- and Z^0-triggers, corresponding to a total integrated luminosity $L = 452\ nb^{-1}$ in the 1982, 1983 and 1984 run periods, is $\sim 2.9 \times 10^6$.

As noted in Ref. [3], a minimum-bias signal obtained from small angle counter hodoscopes [6] was required to occur in coincidence with the W- and Z^0-triggers in order to suppress background from sources other than $\bar{p}p$ collisions.

In the central calorimeter, clusters of energy deposition are obtained by joining all cells which share a common side and contain at least 0.4 GeV. The cluster energy E_{cl} is then defined as $E_{cl} = E_{em} + E_{had}$, where E_{em} is the sum of the energies deposited in the electromagnetic compartments of the calorimeter and E_{had} is the corresponding sum for the hadronic compartments. Two possible values of the cluster energy are retained, depending on whether the calorimeter cluster is considered to result from an electromagnetic shower or from a hadronic shower.

In the two forward calorimeters, clusters are reconstructed as for the central calorimeter. Since the forward calorimeter cells are far from the interaction point, and their size is large compared with that

of an electromagnetic shower, any cluster of electromagnetic origin should consist of at most two adjacent cells. In the case of showers of hadronic origin, the absence of hadronic calorimetry precludes an energy measurement from the calorimeters alone, and information from the momenta of reconstructed charged tracks in the preceding magnetic spectrometer is included. However, the resultant energy resolution remains inferior to that of the central region. In the case of hadronic showers, clustering is allowed to proceed across boundaries of different azimuth, and in addition clustering is allowed across the boundary between the forward and central calorimeters.

We associate jets with energy clusters in the calorimeters. To each jet, j , we associate a momentum $\vec{p}^{j}$ with magnitude equal to the cluster energy, and directed from the event vertex to the cluster centroid. We assume that the jets are massless, and we arbitrarily define a jet as a cluster with transverse energy $E_T > 5$ GeV.

An electron is defined in this analysis as one of the above jets which satisfies in addition a set of basic criteria characteristic of high-p_T electrons:

i. the cluster of energy deposition in the calorimeter must have small lateral dimensions and a small energy leakage in the hadronic calorimeter, as expected for an isolated electron.

ii. a charged particle track which points to the energy cluster must be reconstructed. The pattern of energy deposition in the calorimeter must be consistent with that expected from an isolated electron incident along the track direction.

iii. a hit must have been recorded in the preshower counter (a multi-wire proportional chamber in the central region and proportional tubes in the forward regions, located behind a ~ 1.5 radiation length thick converter), with a pulse height which is large compared with that of a minimum-ionizing particle. The distance of the hit from the track must be consistent with the space resolution of the counter itself. Both these features are characteristic of the early shower developed in the converter by a high-energy electron.

iv. in the two forward regions, where a toroidal magnetic field exists, the charged particle momentum as measured in the spectrometer, and the energy deposition as measured in the calorimeter, must agree within errors.

The momentum, $\vec{p}^{e}$, associated with any electron candidate, takes into account the response of the calorimeter to electrons or photons and the dependence of the calorimeter response to the position and direction of the incident particle.

A quantitative definition of these cuts is given in Table I of Ref. [3], with the following minor differences resulting from an improved understanding of the detector with increased statistics:

i. the energy leakage E_{had} in the hadronic section of the central calorimeter is required to satisfy the condition

$E_{had}/E_{cl} < 0.023 + 0.034\, \ell n\, E_{cl}$, where E_{cl} is the total cluster energy in GeV.

ii. the distance between the hit in the central preshower counter and the track intercept must be less than 10 mm.

iii. the accuracy of track-momentum reconstruction in the forward spectrometers is now measured to be $\delta p = 0.007\, p^2$ (p in GeV/c), whereas a resolution $\delta p = 0.014\, p^2$ (p in GeV/c) was assumed in Ref. [3]. We require, as before, that the track momentum p and the calorimeter energy E must satisfy the condition $|p^{-1} - E^{-1}| / \sigma (p^{-1} - E^{-1}) < 4$.

The corresponding overall efficiencies, η, are estimated to be $\eta = 0.74 \pm 0.04$ and $\eta = 0.79 \pm 0.03$ for the central and forward detectors, respectively.

From the total sample, we find 2436 events which contain at least one cluster having a transverse energy $E_T > 11$ GeV and satisfying all electron identification criteria. The p_T^e distribution of 2444 electron candidates in this event sample is shown in Fig. 1. A shoulder in the region $p_T^e \approx 40$ GeV/c is clearly visible in this distribution. Such a structure is expected from the Jacobian peak which results from the kinematics of $W \to e\nu$ decay.

4. SELECTION OF THE W → eν EVENT SAMPLE

To extract a clean sample of W → eν events from the above sample of 2436 events, we use the fact that W → eν events contain an undetected high-p_T neutrino which is azimuthally separated from the electron, in general, by approximately 180°. On the contrary, fake electrons resulting from misidentified high-p_T hadrons (or jets of hadrons) are expected to be accompanied by another jet at opposite azimuth, having a p_T-value which approximately balances the p_T-value of the fake electron. Such a configuration is typical of events containing high-p_T hadronic jets [7].

As a measure of the fraction of the electron transverse momentum $\vec{p}_T^{\,e}$ which is balanced by jets at opposite azimuth we define the quantity

$$\rho_{opp} = - \vec{p}_T^{\,e} \cdot \Sigma \vec{p}_T^{\,cl} / |\vec{p}_T^{\,e}|^2 \qquad (1)$$

where the sum extends over all clusters (if any) of transverse energy $E_T^{cl} > 3$ GeV which are separated in azimuth from $\vec{p}_T^{\,e}$ by an angle of at least 120°. Most W → eν decays are expected to belong to the category of electron candidates with large p_T imbalance ($\rho_{opp} \approx 0$). On the other hand, for misidentified hadrons or jets of hadrons, we expect large values of ρ_{opp}.

After removing from the sample the 16 events containing a $Z^0 \to e^+e^-$ decay (they will be discussed in Section 11), we subdivide the remaining events into two classes, those with $\rho_{opp} > 0.2$ (1827 events), and those with $\rho_{opp} \leq 0.2$ (593 events). The p_T^e distributions for these two classes of events are shown in Figs. 2a and 2b, respectively. While the distribution of Fig. 2a falls off rapidly with increasing p_T^e, Fig. 2b shows the Jacobian peak structure expected from W → eν decay, which has been strongly enhanced with respect to the inclusive p_T^e spectrum of Fig. 1 by the requirement $\rho_{opp} \leq 0.2$. We note that some W → eν events, in which the decay electron emerges opposite to an associated jet, will fail the ρ_{opp} cut and hence enter Fig. 2a. The efficiency of this cut will be discussed in Section 6.

5. BACKGROUND ESTIMATE TO THE W → eν EVENT SAMPLE

The sample of electron candidates having $\rho_{opp} \leq 0.2$ is still contaminated by two-jet or multi-jet events in which one of the jets is misidentified as an electron and at least one jet escapes detection (either totally or partially) because of the incomplete angular coverage of the apparatus.

To estimate the background to the signal of W → eν decays we follow the method outlined in Ref. [3] which assumes that none of the electron candidates in the events having $\rho_{opp} > 0.2$ (Fig. 2a) result from W → eν decays. Most electron candidates in this sample are, of course, misidentified hadrons or jets of hadrons. From the sample of events containing at least one energy cluster with $E_T > 11$ GeV we extract a sample of events for which the main features of the cluster (lateral dimensions, energy leakage into the hadronic calorimeter, absence of charged particle tracks pointing to it, and presence of an isolated conversion signal in the preshower counter) are consistent with an isolated high-p_T π^0. These events (hereafter referred to as the background sample) are then analysed in exactly the same way as the sample of electron candidates. In particular, they are subdivided into two classes corresponding to $\rho_{opp} > 0.2$ and $\rho_{opp} \leq 0.2$.

As shown in Fig. 2a, we find that for $\rho_{opp} > 0.2$ the p_T-distributions of the background and candidate electron samples have similar shapes. In each bin of p_T, we obtain the background contribution B to the electron candidates having $\rho_{opp} \leq 0.2$ from the formula :

$$B = (N_e/N_{bkgd})\, n_{bkgd} \qquad (2)$$

where N_e (N_{bkgd}) is the total number of electron (background) candidates having $\rho_{opp} > 0.2$, and n_{bkgd} is the number of background events with $\rho_{opp} \leq 0.2$.

The background spectrum $B(p_T)$ so obtained is shown in Fig. 2b as a dotted curve. It accounts for most of the electron candidates in the p_T^e range between threshold and ~ 20 GeV/c. However, for $p_T^e > 25$ GeV/c, the histogram of Fig. 2b contains 119 events, whereas the integral of $B(p_T)$ gives only 5.8 ± 1.7 events.

The 119 events represent an almost pure sample of $W \rightarrow e\nu$ events. For each event the neutrino transverse momentum, $\vec{p}_T^{\,\nu}$, is defined to be equal to the missing transverse momentum, $\vec{p}_T^{\,miss}$, which is obtained from the expression

$$\vec{p}_T^{\,miss} = - \vec{p}_T^{\,e} - \Sigma \vec{p}_T^{\,j} - \lambda \vec{P}_T^{\,sp} \qquad (3)$$

where the sum extends over all observed jets, j. The vector $\vec{P}_T^{\,sp}$ is the total transverse momentum carried by the system of all other particles not belonging to jets. The correction factor λ takes into account both the incomplete detection of the rest of the event, and the nonlinearity of the calorimeter response to low energy particles. We obtain the value $\lambda = 1.5 \pm 0.6$ by minimising $<|\vec{p}_T^{\,miss}|>$ for the sample of Z^0 events observed in the experiment (see Section 13).

Fig. 3a shows all the electron candidates having $p_T^e > 11$ GeV/c in the (p_T^e, p_T^ν) plane. The region populated by the $W \rightarrow e\nu$ signal, for which one expects $p_T^\nu \approx p_T^e$, is clearly visible in this plot. Figure 3b shows the same distribution after the selection $\rho_{opp} \leq 0.2$.

6. CROSS-SECTION FOR INCLUSIVE W PRODUCTION

We obtain the cross-section σ_W^e for the inclusive process $\bar{p}p \rightarrow W^\pm$ + anything followed by the decay $W \rightarrow e\nu$ from the relation

$$N_W^e = L \, \sigma_W^e \, \varepsilon \, \eta \qquad (4)$$

where N_W^e is the observed number of $W \rightarrow e\nu$ decays, L is the total integrated luminosity, ε is the detector acceptance (which includes the effect of the p_T^e threshold), and η is the overall efficiency of the electron identification criteria averaged over the central and forward detectors.

The detector acceptance ε is calculated by Monte Carlo simulation. The effect of the cut $\rho_{opp} \leq 0.2$, which rejects electrons in the presence of hadron jets at opposite azimuthal angles, is taken into account by generating events which contain $W \rightarrow e\nu$ decays and jets, using a QCD-inspired Monte Carlo program [8]. For data collected at $\sqrt{s} = 546$ GeV, this cut rejects $(5 \pm 2)\%$ of $W \rightarrow e\nu$ decays for which $p_T^e > 25$ GeV/c. The corresponding number at $\sqrt{s} = 630$ GeV is $(7 \pm 2)\%$; the quoted uncertainty reflects the measurement accuracy of low-E_T clusters of energy in the calorimeter.

We obtain N_W^e from the event sample satisfying $p_T^e > 25$ GeV/c. This sample is contaminated by fake electrons, as discussed in Section 5, as well as by electrons from $Z^0 \rightarrow e^+e^-$ decay with one electron escaping the acceptance, and from $W \rightarrow \tau\nu_\tau$ followed by $\tau \rightarrow e\nu_e\nu_\tau$.

The Z^0 contribution is estimated by a Monte Carlo simulation, whose result is normalised to the total number of $Z^0 \rightarrow e^+e^-$ decays observed in this experiment.

The number of electrons from the $W \rightarrow \tau\nu_\tau$, $\tau \rightarrow e\nu_e\nu_\tau$ decay chain, N_τ^e, is given by

$$N_\tau^e = (N_W^e/\varepsilon)\, \varepsilon_\tau\, B_\tau \qquad (5)$$

where ε_τ is the detector acceptance for electrons from the $W \rightarrow \tau \rightarrow e$ decay chain, and $B_\tau = 0.17$ is the branching ratio for the decay $\tau \rightarrow e\nu_e\nu_\tau$ [9]. A Monte Carlo simulation gives $\varepsilon_\tau = 0.10 \pm 0.01$, where this value includes the effect of the cut $p_T^e > 25$ GeV/c.

Lists of the various contributions to the observed numbers of electron candidates with $p_T^e > 25$ GeV/c, as well as of the values of L, ε and η (see Eq. 4), are given separately in Table I for the two values of $\sqrt{s}$ at which the data have been collected. We note that the value of L for $\sqrt{s} = 546$ GeV differs by ~ 8% from that given in Ref. [3] as a result of a recent and more precise measurement of the $\bar{p}p$ total non-diffractive cross-section [6] at $\sqrt{s} = 546$ GeV. The corresponding value at $\sqrt{s} = 630$ GeV has been obtained by extrapolation. The quoted error on L, of $\pm$ 8%, reflects the uncertainty of the non-diffractive cross-section, and uncertainties in the monitoring of the luminosity.

The sum of all contributions to the 119 events with $p_T^e > 25$ GeV/c is shown in Fig. 2b for $M_W = 81.2$ GeV (see Section 7).

From the quantities given in Table I we derive the values

$$\sigma_W^e(546 \text{ GeV}) = 0.50 \pm 0.09 \text{ (stat.)} \pm 0.05 \text{ (syst.) nb} \quad (6)$$

$$\sigma_W^e(630 \text{ GeV}) = 0.53 \pm 0.06 \text{ (stat.)} \pm 0.05 \text{ (syst.) nb} \quad (6')$$

The quoted systematic uncertainty includes contributions from uncertainties on L, the ρ_{opp} cut, the electron identification efficiency, and the detector acceptance. The corresponding theoretical predictions [11] are $\sigma_W^e = 0.36^{+.11}_{-.05}$ and $0.45^{+.14}_{-.08}$ nb respectively, where the errors reflect theoretical uncertainties, that result in part from experimental uncertainties of the structure-function measurements, and in part from higher-order QCD contributions. The data are also consistent with recent results from the UA1 Collaboration [10].

The increase of the W production cross section between the two $\sqrt{s}$ values is measured to be

$$r = \sigma_W^e(630 \text{ GeV})/\sigma_W^e(546 \text{ GeV}) = 1.06 \pm 0.23 \text{ (stat)} \quad (7)$$

This value, which has a small systematic uncertainty, agrees with the prediction [11] $r = 1.26$ which is practically free of theoretical uncertainties.

7. DETERMINATION OF THE W MASS

A value of the W mass, M_W, can be obtained from the electron candidates with $\rho_{opp} \leq 0.2$ using two methods :

i. the p_T^e distribution of Fig. 2b is compared with that expected from $W \rightarrow e\nu$ decay for the 119 events containing an electron candidate of $p_T^e > 25$ GeV/c,

ii. for each event we define a transverse mass, M_T, such that $M_T^2 = 2\, p_T^e\, p_T^\nu\, (1 - \cos\Delta\phi)$, and $\Delta\phi$ is the azimuthal separation between $\vec{p}_T^{\,e}$ and $\vec{p}_T^{\,\nu}$. Fig. 4 shows the M_T-distribution for 119 events of Fig. 2b containing an electron candidate of $p_T^e > 25$ GeV/c Superimposed on Fig. 4 is the expected distribution of M_T for $W \rightarrow e\nu$ decay, and as well the summed contribution of other processes.

A Monte Carlo program is used to generate the distributions dn/dp_T^e and dn/dM_T for different values of M_W. The W longitudinal momentum distribution is obtained from the quark structure functions of the proton as parametrised by Glück et al. [12]. The W transverse momentum, p_T^W, is generated from the predicted QCD shape of Altarelli et al. [11]. The decay is described by the standard V-A coupling, and a fixed value of the W width, $\Gamma_W = 3$ GeV, is used. The calorimeter response to electrons is also taken into account. Finally, the requirement $\rho_{opp} \leq 0.2$, which rejects electrons in the presence of jets at opposite azimuthal angles, distorts the p_T^e and M_T distributions by eliminating a fraction of the W's produced in association with high-p_T jets. In particular, the distortion to the p_T^e spectrum is large when $p_T^e > M_W/2$. This has been studied using the QCD Monte Carlo program mentioned previously [8], and p_T^e-dependent (or M_T-dependent) correction factors have been applied to the generated distributions.

The best fits to the experimental distributions are:

$$M_W = 80.6 \pm 1.1 \text{ (stat.) GeV/c}^2 \quad \text{(from the } p_T^e \text{ spectrum)}$$

$$M_W = 81.2 \pm 1.0 \text{ (stat.) Gev/c}^2 \quad \text{(from the } M_T \text{ spectrum).}$$

The backgrounds discussed in Section 6 have a negligible effect on the mass evaluation, since they are dominantly at small p_T^e or M_T, and the best fit value of M_W depends mainly on the shape of the distributions at large values of p_T^e or M_T. We have checked that by making strict electron-identification selections, which result in a small background at the expense of electron efficiency, the best fit mass is unchanged.

Additional systematic errors result from theoretical uncertainties on Γ_W and $<p_T^W>$, and from experimental uncertainties. The latter category includes the p_T^e-dependence of the ρ_{opp} cut efficiency, the uncertainty of the parameter λ defined in Section 5, and calorimeter calibration uncertainties. The contributions of each of these uncertainties to the systematic error on the determination of M_W are summarised in Table II.

The main contribution to the total systematic error arises from the uncertainty of $\pm 1.6\%$ on the mass scale, discussed in Section 2. We choose to separate this error because it cancels in the ratio M_W/M_Z. The remaining systematic uncertainties for the fit to the p_T^e-spectrum result mainly from $<p_T^W>$ and the ρ_{opp} cut, and when summed in quadrature amount to ± 0.8 GeV/c^2. The remaining systematic uncertainties for the fit to the M_T-spectrum amount to ± 0.5 GeV/c^2, mainly due to uncertainties in the measurement of p_T^ν. Although the two methods give consistent results, we quote the result of the latter method because of its smaller systematic uncertainty of ± 0.5 GeV/c^2, which we add in quadrature to the statistical error. To summarise:

$$M_W = 81.2 \pm 1.1 \text{ (stat.)} \pm 1.3 \text{ (syst.) GeV/c}^2. \qquad (8)$$

Within errors, this value agrees with our previous result [3], and with the 1983 data of UA1 [13].

We note that a fit to the M_T distribution of Fig. 4 using the W width, Γ_W, as a second free parameter provides a way to determine Γ_W. We obtain the upper limit $\Gamma_W < 7$ GeV/c^2 at the 90% confidence level.

8. SEARCH FOR $W \to e\nu$ DECAYS IN A SAMPLE OF EVENTS WITH LARGE MISSING TRANSVERSE MOMENTUM

A search for events with large missing transverse momentum (p_T^{miss}) has been performed in the UA2 experiment [14] to identify events containing high-p_T jets or photons produced in association with large p_T^{miss}. Such events have been reported by the UA1 Collaboration [15]. The final sample of events is expected to contain $W \to e\nu$ decays, and it is therefore possible to cross-check the W-selection of Section 4 using an independent analysis.

Events of large p_T^{miss} were selected using a trigger such that p_T^{miss} exceeded 30 GeV/c. This signal was constructed by hardware using the transverse energies measured in the cells of the central calorimeter only. The trigger was operational only during the 1984 run ($\sqrt{s}$ = 630 GeV, L = 310 nb^{-1}).

A major background contribution to the p_T^{miss} trigger results from beam-halo particles appearing as an accidental overlap with a minimum-bias $\bar{p}p$ interaction. As described in [14], the majority of this background is removed by requiring valid timing of both the small-angle counter hodoscopes, and a large forward veto-counter array.

At the analysis level, the p_T^{miss} requirement of the trigger is repeated, using more accurate calorimeter calibrations and a knowledge of the event vertex. In addition, we require:

i. $|\Sigma \vec{p}_T^{cl}| > 30$ GeV/c, with $p_T^{cl} > 3$ GeV/c,

ii. $\Sigma |\vec{p}_T^{cl}| < 10$ GeV/c with $p_T^{cl} > 3$ GeV/c, in a wedge of $\pm$ 60° opposite in azimuth to the cluster selected as an electron candidate, and no energy cluster of $E_T > 3$ GeV in this angular range in the forward calorimeters.

In the subsequent analysis we apply calorimeter requirements on the selected cluster of the central calorimeter, as in Section 3. That is, we require that the energy cluster has small lateral extension and

limited energy leakage in the hadronic compartment of the calorimeter. To further reduce the beam-halo background, we require that less than 50 % of the energy of the selected cluster is deposited in edge cells of the calorimeter, and we exclude long clusters in the calorimeters that are parallel to the beam line and characteristic of beam halo interactions. A total of 63 events survive the calorimeter selection with $p_T^e > 30$ GeV/c and $p_T^{miss} > 30$ GeV/c.

In addition to $W \to e\nu$ events, the sample still contains background from beam-halo interactions and from two-jet events in which one jet escapes detection due to the incomplete angular coverage of the apparatus. Using the method described in [14], the background contributions are estimated to be 2.3 ± 1 and 6.5 ± 1 events respectively. Fig. 5 shows the p_T^{miss} distribution of the events, and the two-jet background contribution. The expected Jacobian peak for $W \to e\nu$ decay is visible.

Of the 63 events, 51 events satisfy $p_T^{miss} > 34$ GeV/c, where the trigger is fully efficient. A total of 30 events in this sample are also found in the electron search of previous sections. An additional ten events compatible with $W \to e\nu$ decay were identified by scanning at a high-resolution graphic display, and this number is consistent with the efficiency for electron identification quoted in Table I. After including background contributions, a total of 46 ± 7 events are expected in the event sample, compared with 51 events actually observed.

From the 51 events satisfying $p_T^{miss} > 34$ GeV/c, we evaluate the cross-section, σ_W^e, using an analysis which is based solely on calorimeter information. The result, $\sigma_W^e = 0.52 \pm 0.09$ (stat) nb, agrees with the value (6') obtained from the electron search, and with the preliminary result of [14].

9. CHARGE ASYMMETRY

At the energies of the CERN $\bar{p}p$ Collider, W production is dominated by $q\bar{q}$ annihilation involving at least one valence quark or antiquark. As a consequence of V-A coupling, the W is

produced with almost full polarisation along the direction of the incident $\bar{p}$ beam, and a distinctive charge asymmetry can be observed in the decay $W \rightarrow e\nu$.

If θ^* is the angle between the charged lepton and the direction of the incident proton in the W rest frame, the angular distribution has the form

$$dn/d(\cos\theta^*) \propto (1-q\cos\theta^*)^2 + 2q\alpha\cos\theta^* \qquad (9)$$

where $q = -1$ for electrons and $+1$ for positrons. The parameter α, with the property $0 \leq \alpha \leq 2$, depends on the ratio x between the A and V couplings (time reversal invariance requires x to be real). Under the assumption that x is the same for both $Wq\bar{q}$ and $We\nu$ couplings, α is given by

$$\alpha = [(1-x^2)/(1+x^2)]^2. \qquad (10)$$

For standard V-A coupling α is zero. We note, however, that the angular distribution given by Eq. (9) provides no information on either the sign of x, or on the choice of x or 1/x.

In the UA2 detector a determination of the sign of the electron charge is only possible in the forward detectors, where a magnetic field is present. Since the sensitivity of the data to the exact form of the angular distribution is highest for values of $\cos\theta^*$ close to ± 1, corresponding to small values of p_T^e, we consider all electron candidates with $p_T^e > 20$ GeV/c and $\rho_{opp} \leq 0.2$ that are detected in the forward regions.

This sample contains 28 events with an estimated background of 2 events. A comparison between the electron momentum p and the energy E, as measured in the calorimeter, is made in Fig. 6. This figure shows the position of these events in the plane $(\hat{p}^{-1}, E^{-1})$, where $\hat{p}$ is the momentum with the sign of $q.\cos\theta_e$ (θ_e being the laboratory angle of the electron with respect to the proton direction). The horizontal error bars in Fig. 6 represent the uncertainty on the measurement of p^{-1}, which is 0.007 $(GeV/c)^{-1}$. There are 20 events in the region of negative $\hat{p}$ values (the region favoured by the V-A coupling), and 8 events in the region of positive $\hat{p}$ values, corresponding to an asymmetry of

0.43 ± 0.17. This value is in good agreement with the expected asymmetry for V-A coupling of 0.53 ± 0.06 ($\alpha = 0$ in Eq. 9), as obtained by a Monte Carlo calculation which takes into account the expected sea-quark contribution, and as well a background contribution which is estimated to include 0.6 events from $Z^0 \rightarrow e^+e^-$ decay with one of the two electrons undetected and 0.3 events resulting from $W \rightarrow \tau\nu$ decay.

To extract a value of α from these data we use a Monte Carlo program to compare the expected two-dimensional distributions $f^{\pm}(p_T^e, \theta_e)$, for positrons and electrons separately, with those observed. To each event we assign a likelihood $Q_i = f^+\eta^+ + f^-\eta^-$, where $\eta^+(\eta^-)$ is the probability that the observed particle was a positron (an electron). The functions $f^{\pm}$ take into account the W motion, and the probabilities $\eta^{\pm}$ include the uncertainty of the charge sign determination resulting from the momentum measurement error.

After taking into account biases of the maximum - likelihood estimator, we measure α to be consistent with zero, as expected for V - A coupling. We determine $\alpha < 0.39$ (68% confidence level), corresponding to $0.48 < |x| < 2.1$ (see Eq. 10).

We use the sample of $W \rightarrow e\nu$ candidates with $p_T^e > 25$ GeV/c (119 events) to measure the charge-averaged $\cos\theta^*$ distribution, which has the form $dn/d(\cos\theta^*) \propto 1+\cos^2\theta^*$ if only vector and axial-vector couplings are involved (see Eq. 9). A unique value of $\cos\theta^*$ for each event is not calculable because the neutrino longitudinal momentum, p_L^{ν}, is not measured experimentally, and the condition that $M_{e\nu} = M_W$ results in two solutions for p_L^{ν}. For events in which both solutions are physically allowed, we choose the solution corresponding to the smaller absolute value of the W longitudinal momentum, p_L^W. Events for which $M_T > M_W$ are excluded from this analysis because in this case both solutions are unphysical.

Transforming the electron four-momentum to the W rest frame provides a unique value of θ^* only if $p_T^W = 0$, and the quarks have no transverse momentum. For $p_T^W \neq 0$ the initial parton directions are not known and the Collins-Soper [16] convention is used.

We use a Monte Carlo program to correct the $\cos\theta^*$ distribution for the effects of the detector acceptance and resolution. The corrected $|\cos\theta^*|$ distribution shown in Fig. 7 is consistent with the expected form $1 + \cos^2\theta^*$, modified to take into account higher-order QCD contributions to W-production.

10. LONGITUDINAL MOMENTUM DISTRIBUTION OF THE W

The fractional beam momentum $x_W = 2p_L{}^W/\sqrt{s}$ carried by the W bosons can be used, via the relations

$$x_W = x_p - x_{\bar{p}}, \quad \text{and} \tag{11}$$

$$M_W{}^2/s \cong x_p x_{\bar{p}} \quad (\text{for } p_T{}^W \ll M_W) \tag{11'}$$

to determine the fractional momenta of the partons involved in W production. The distributions dn/dx_p and $dn/dx_{\bar{p}}$ are expected to be identical, and, at the energies of the CERN $\bar{p}p$ Collider, the partons involved are mostly quarks (antiquarks) in the proton (antiproton).

Fig. 8a shows the distribution $dn/dx = dn/dx_p + dn/dx_{\bar{p}}$, as determined for the 1982-83 event sample ($\sqrt{s}$ = 546 GeV). The corresponding distribution for the 1984 event sample ($\sqrt{s}$ = 630 GeV) is shown in Fig. 8b. Superimposed are the expected distributions from Ref. [8], distorted by the effects of the detector acceptance and resolution.

11. ELECTRONS WITH ASSOCIATED JETS OF LARGE TRANSVERSE MOMENTUM

Non-leading QCD contributions to W production have been discussed in a large number of theoretical papers [11,17]. The main consequences of these contributions are to increase the production cross-section by ~30%, and to give the W a sizeable average transverse momentum p_T^W. Furthermore, for relatively large values of p_T^W, the W bosons are expected to recoil against hadronic jets which can be observed experimentally.

In the sample of $W \rightarrow e\nu$ events which was used in the previous Sections, the requirement $\rho_{opp} \leq 0.2$ was applied to reduce the background of fake electrons. However, this requirement rejects electrons in the presence of jets at opposite azimuthal angles. As seen from Fig. 3a, a strong background suppression is also obtained by requiring that the missing transverse momentum (p_T^{miss} or p_T^{ν}) exceeds 25 GeV/c, independent of the azimuthal separation between $\vec{p}_T^{\,e}$ and $\vec{p}_T^{\,\nu}$.

A total of 807 events from the 1983 and 1984 Collider runs (an integrated luminosity $L = 436\ nb^{-1}$) contain an electron candidate of $p_T^e > 15$ GeV/c. Fig. 9a shows the distribution of these events in the (p_T^{ν}, E_T^J) plane, where E_T^J is defined as the summed transverse energy of all reconstructed jets (if any) in the event. As noted in Section 3, each constituent jet, j, of the system J must have a transverse energy $E_T > 5$ GeV.

The results of an analysis with the $p_T^{\nu} > 25$ GeV/c requirement applied to the 1983 data have already been published [18]. In this Section, we repeat the analysis with the enlarged data sample. The use of Eq. (3) to calculate p_T^{ν}, and the implementation of a 5 GeV transverse energy threshold to define jets (it was 3 GeV in [18]), represent small modifications to the previous analysis. In Ref. [18], most events were consistent with W production from standard QCD processes. However, the sample contained three events (A, B, and C in [18]) in which an $e\nu$ pair consistent with W decay was observed in association with very hard jets, under low background conditions. Two of these events (B and C) were not easily interpreted in terms of standard QCD processes because of their large measured values

of E_T^J and their large p_T^ν values ($p_T^\nu > 50$ GeV/c). These events suggested the existence of a new unexpected phenomenon, and in the 1984 data sample about nine additional events satisfying $p_T^e > 15$ GeV/c, $p_T^\nu > 50$ GeV/c and $E_T^J > 30$ GeV (as for events A, B and C) could have been expected. With the enlarged data sample, no additional event satisfying $p_T^\nu > 50$ GeV/c is observed, making the interpretation of events B and C in terms of some new phenomenon less likely. We note that no instrumental differences which may have changed the performance of the detector between the 1983 and 1984 runs have been found.

The background evaluation follows the method described in Section 5. We consider a sample of events for which the electron is replaced by a neutral particle (or system of particles) whose behaviour in the detector is consistent with that of an isolated π^0 having $p_T > 15$ GeV/c. The distribution of these background events in the (p_T^ν, E_T^J) plane is shown in Fig. 9b. To estimate the background contribution from hadrons or hadron jets that are misidentified as electrons, we assume that the electron candidates having $p_T^e < 20$ GeV/c, $p_T^\nu < 20$ GeV/c are all misidentified hadrons, and we normalize the plot of Fig. 9b to the number of events in the same region. The renormalised number of background events is then assumed to represent a correct background estimate for all regions of the (p_T^ν, E_T^J) plane. We have checked that the renormalisation of the background is within statistics independent of p_T^ν and p_T^e. Fig. 10 shows the p_T^ν distribution for all electron events, together with the background estimate of 10.6 ± 2.0 events in the region $p_T^\nu > 25$ GeV/c. This distribution shows the Jacobian peak at $p_T^\nu \approx 40$ GeV/c as expected for $W \to e\nu$ decay.

Of the 7 events observed with $p_T^\nu > 25$ GeV/c and $E_T^J > 30$ GeV, three events (A, B and C) are from the 1983 run. The corresponding background of fake electrons is estimated to be 2.3 ± 0.7 events in this sample. Only these three events satisfy $p_T^\nu > 50$ GeV/c, $E_T^J > 30$ GeV, and the corresponding background is estimated to be < 1.1 events (90% confidence level). Two of the 7 events have a different configuration from the others, and are incompatible with the decay $W \to e\nu$. These events have been discussed elsewhere [19]. The remaining events (A, B, C, and two events of the

1984 run) are all characterised by a large azimuthal separation between the electron and the neutrino ($\Delta\phi > 120^0$). The $e\nu$ pairs have transverse mass values that are consistent with the M_T distribution from $W \rightarrow e\nu$ decay that is shown in Fig. 4, and we therefore assume that these events consist of W bosons produced in association with hadronic jets.

Following the analysis of [18], we note that the probability, $P_W(J)$, for a W to be produced in association with a jet or system of jets, J, is independent of the W decay mode. It can be evaluated, for example, using events for which the W decays in hadronic jets j_1 and j_2. In practice, however, the majority of events kinematically consistent with the decay of W into two jets result from QCD processes not involving W production. Because of the larger number of relevant sub-processes, we would expect larger values of $P_{j_1j_2}(J)$ for QCD processes. We therefore expect to obtain an upper limit to $P_W(J)$ from an evaluation of the fraction $P_{j_1j_2}(J)$ of events containing 2 jets j_1 and j_2, which also contain an additional jet or system of jets, J. The fraction $P_{j_1j_2}(J)$ has been evaluated separately for data of 1983 and 1984, because of the different $\sqrt{s}$-value [20]. We retain only those (j_1j_2) pairs that satisfy the same kinematic cuts as $e\nu$ pairs from W-decay, and with an invariant mass experimentally compatible with what would be measured in the apparatus from the decay of W into 2 quark jets. An identical treatment of the j_1j_2 and $e\nu$ systems is not possible because, contrary to the electron and neutrino, j_1 and j_2 are measured only in the central calorimeter because of the hardware trigger criteria used for the jet sample. However, this results in only a small correction to $P_{j_1j_2}(J)$.

The fraction $P_{j_1j_2}(J)$ may be evaluated as a function of any set of parameters describing the kinematic configuration of the J system. In Ref. [18], parameters appropriate to each event configuration were selected. However, since no additional events in the kinematic region of A, B and C were identified during the 1984 run, we now prefer to evaluate $P_{j_1j_2}(J)$ as the function of a common parameter independent of the special configuration of individual events.

We use the function $F_{j_1j_2}(E_T^0)$, defined by the probability that a j_1j_2 pair is associated with a system J having $E_T^J > E_T^0$. In Fig. 11a, we compare $F_{j_1j_2}(E_T^0)$ with the corresponding function,

$F_W(E_T^0)$, of $W \to e\nu$ events for which the electron is detected in the central calorimeter. We note that:

i. the choice of E_T^J in estimating $F_{j_1 j_2}(E_T^0)$ is conservative. By instead choosing E_T^j, corresponding to the jet of largest E_T in the system J, the corresponding values of $F_{j_1 j_2}(E_T^0)$ would be reduced by a factor of between two and five for the E_T^0 range 35 to 65 GeV.

ii. the events B and C remain outstanding in the 1983 data sample (Fig. 11b). From their associated $F_{j_1 j_2}(E_T^0)$-values, only 0.07 events could be expected. When combined with the 1984 data, that upper limit increases to ~ 0.3 events. More data are necessary to ascertain whether the events B and C result from QCD processes. However, the absence of such events during the 1984 run strongly suggests that interpretation.

Assuming that the events discussed above are $W \to e\nu$ events for which the W is produced via conventional QCD processes, the data sample may be compared with the predictions of the Monte Carlo program [8] which generates W bosons with or without hard jets according to perturbative QCD up to $O(\alpha_s^2)$. This program, which includes a full simulation of the UA2 detector, was used to predict the associated production of W bosons with jets of $E_T > 5$ GeV. For large E_T (in excess of about 10 GeV), where pertubative QCD evaluations are appropriate and the energy response of the calorimeter to jets is well understood, the simulation should provide a reliable description of the data. Uncertainties of the theoretical predictions include the choice of the structure functions used, and the assumed value of α_s [21].

This program is used to predict the fraction $F_W(E_T^0)$, and the result is superimposed on Fig. 11a, for α_s-values in the range 0.14 to 0.20. The evaluated $F_W(E_T^0)$ - values are in qualitative agreement with data from the 1984 run, but for the reasons discussed above, that agreement is less good when data from the 1983 run are included. Multiplying the theoretical value of $F_W(E_T^0)$ by the

number of events satisfying $p_T^e > 15$ GeV/c and $p_T^\nu > 25$ GeV/c, we obtain an estimate of the expected number of $W \to e\nu$ events produced in association with jets having $E_T^J > E_T^0$ from standard QCD processes. For $\alpha_s = 0.14$, this number is 2.5 ± 0.3 events for $E_T^0 = 30$ GeV, to be compared with five events observed.

12. EVENT STRUCTURE ASSOCIATED WITH W - PRODUCTION

We now consider the total data sample satisfying $p_T^e > 15$ GeV/c and $p_T^\nu > 25$ GeV/c, and we compare this sample with the expectations of conventional QCD processes for W-production. After applying a cut on the transverse mass, $M_T > 20$ GeV/c^2, the sample contains 126 events.

Fig. 12 shows the distribution of the W transverse momentum p_T^W, defined as $\vec{p}_T^W = \vec{p}_T^e + \vec{p}_T^\nu$. A QCD prediction of Altarelli et al. [11], illustrated by the curve of Fig. 12, is in good agreement with the data. Also shown is the prediction of Ellis et al. [8]. For $p_T^W > 30$ GeV/c we expect about 2.7 events to be compared with 6 observed events and an estimated background of 0.7 events. Given the theoretical uncertainties of the QCD prediction, the agreement is reasonable. The average value of p_T^W for the distribution of Fig. 12 is $\langle p_T^W \rangle = 8.8 \pm 1.7$ GeV/c. The quoted error on $\langle p_T^W \rangle$ mainly results from the uncertainty in measuring the correction factor λ that is used in the evaluation of p_T^ν (see Section 5).

In Fig. 13, we show the E_T spectrum of the jet system J. Again, the superimposed Monte Carlo expectations are in good agreement with the data, for $E_T^J > 10$ GeV.

For each event of the W-sample which has an associated jet system J, we assume that the $e\nu$ pair results from W-decay, and we evaluate the invariant mass M($e\nu$J) corresponding to the minimum longitudinal momentum of the W - J system. The resulting M(WJ) distribution is shown on Fig. 14, with superimposed Monte Carlo expectations [8] that are in reasonable agreement with the data.

The same event sample is used to compare the "underlying event" that is obtained after excluding the electron from the W-decay, with the characteristics of minimum-bias events. To remove expected differences from QCD hard processes, only those events having no associated jet are considered. In Fig. 15 we compare the quantity $\tilde{E}_T$ which is defined as the summed transverse energy of all particles in the underlying event, in the pseudo-rapidity range $|\eta| < 1$. We measure :

$$<\tilde{E}_T> = 8.0 \pm 0.6 \text{ GeV} \qquad (W \to e\nu \text{ events with no jet})$$

$$<\tilde{E}_T> = 6.5 \pm 0.3 \text{ GeV} \qquad (\text{minimum-bias events with no jet}).$$

In the case of the minimum-bias event sample, the quoted error reflects the uncertainty due to run-by-run variations of $<\tilde{E}_T>$. It should be noted that the differences observed between the underlying event structure of the W-sample, and that of minimum-bias events, are sensitive to the E_T-threshold used to define the jets. We also note that 2.3% of minimum-bias events have at least one associated jet of $E_T > 5$ GeV in the pseudo-rapidity range $|\eta| < 1$.

The associated charged particle multiplicity is compared in Fig. 16 for the same events. The plotted quantity is the experimentally measured transverse-track multiplicity, N_{ch}, in the pseudo-rapidity interval $|\eta| < 1.7$, before corrections for track efficiency, spurious tracks etc. We measure :

$$<N_{ch}> = 19.5 \pm 1.3 \qquad (W \to e\nu \text{ events with no jet})$$

$$<N_{ch}> = 14.7 \pm 0.3 \qquad (\text{minimum-bias events with no jet}).$$

13. THE DECAY $Z^0 \to e^+e^-$

The observation of seven $Z^0 \to e^+e^-$ decays and one $Z^0 \to e^+e^-\gamma$ decay among the data collected during the 1982-83 Collider runs has already been reported [2,3]. We first describe the search for events containing two high-p_T electrons among a sample of $\sim 1.1 \times 10^6$ Z^0 triggers recorded during the 1984 run. We then discuss the full data sample.

The efficiency of the electron identification criteria is 0.74 ± 0.04 in the central region and 0.79 ± 0.03 in the forward regions (see Section 3), and therefore the requirement that both electrons satisfy these criteria would reject approximately one half of all $Z^0 \rightarrow e^+e^-$ decays. To avoid this loss, we prefer to use less selective but more efficient criteria.

A first selection is made by keeping only the events which contain at least two energy clusters of $E_T > 5$ GeV passing the calorimeter cuts used in the electron analysis (see Section 3). A total of 1154 events having a two-cluster invariant mass, M_{ee}, above 20 GeV/c^2 survives this requirement. The M_{ee} distribution of these events is shown in Fig. 17a. Although these criteria are rather loose, an accumulation of events in the region of the Z^0 mass is already visible at this stage of the analysis.

The additional requirement that at least one cluster satisfies all electron identification criteria selects 54 events, whose M_{ee} distribution is shown in Fig. 17b. There is a clear peak consisting of 8 events with a mass value in excess of 75 GeV/c^2, well separated from the rapidly falling continuum at lower mass values.

To estimate the background contribution from two-jet final states to the M_{ee} distributions of Figs. 17a and 17b, we use the original sample of events selected by the Z^0-trigger, which consists mostly of two-jet events, and we measure the probability that a jet passes a given set of electron cuts. We then verify experimentally that the fraction of events for which both jets pass the cuts is given by the square of this probability in the mass region $20 < M_{ee} < 70$ GeV/c^2. This fraction is found to be approximately independent of M_{ee} for $M_{ee} > 40$ GeV/c^2.

By applying this method to the region $M_{ee} > 70$ GeV/c^2 we estimate that the contribution of two-jet events to the distribution of Fig. 17a is 3.8 ± 0.4 events, compared with 13 observed events. In the same mass range the background contribution to the distribution of Fig. 17b is 0.21 ± 0.02 events, compared with an observed number of 8 events. In 4 of the 8 events, the second cluster also satisfies all electron-identification criteria. In the remaining events, the second cluster is compatible with an

electron, given the quoted efficiencies for electron identification. We conclude that our final selection criteria lead to a background-free sample of $Z^0 \to e^+e^-$ decays, while being at the same time $(89 \pm 3)\%$ efficient.

Fig. 18 shows the mass values and the measurement errors for the eight events with $M_{ee} > 70$ GeV/c^2, together with those of the eight events from the 1982-83 Collider runs. We note that the mass values of the 1982-83 events have undergone small changes with respect to our previous publication [3] following a recalibration of the calorimeter response as a function of the impact point. In particular, in one event (called F in Refs. 2 and 3), an apparent inconsistency between the calorimeter energy pattern for one of the two electrons and the impact point of the track is now understood to have resulted from the increase of the light attenuation in the scintillator as a function of time. As a consequence, the 1982-83 sample now contains five well-measured events instead of four.

A list of parameters for the full sample of 16 events is given in Table III. We obtain a value of the Z^0 mass by fitting the mass values of these events, with the exclusion of events Z1, Z3 and Z5 (these events are denoted as D, G, and H in Refs. 2 and 3), to a relativistic Breit-Wigner shape modified by the experimental mass resolution. The result is

$$M_Z = 92.5 \pm 1.3 \text{ (stat.)} \pm 1.5 \text{ (syst.) GeV/}c^2 \qquad (12)$$

where the systematic error reflects the $\pm$ 1.6% uncertainty on the absolute energy scale of the calorimeter.

The cross-section for Z^0 production followed by the decay $Z^0 \to e^+e^-$, σ_Z^e, can be obtained from the observed number of events after taking into account the detector acceptance (57% at $\sqrt{s} = 546$ GeV and 55.5% at $\sqrt{s} = 630$ GeV as estimated by a Monte Carlo simulation), the efficiency of the identification criteria, and the integrated luminosity. We find

$$\sigma_Z^e(546 \text{ GeV}) = 110 \pm 39 \text{ (stat.)} \pm 9 \text{ (syst.) pb} \qquad (13)$$

$$\sigma_Z^e(630 \text{ GeV}) = 52 \pm 19 \text{ (stat.)} \pm 4 \text{ (syst.) pb.} \qquad (13')$$

Within the large statistical errors, both values are consistent with theoretical predictions [11], which give $\sigma_Z^e = 42^{+13}_{-6}$ pb, and $\sigma_Z^e = 51^{+16}_{-10}$pb at $\sqrt{s} = 546$ and $\sqrt{s} = 630$ GeV, respectively.

Fig. 19 shows the distribution of the Z^0 transverse momentum, p_T^Z, for all 16 events. The result of a QCD calculation [11], normalised to the observed number of events for $p_T^Z < 15$ GeV/c, is also shown in Fig. 19. The average value of p_T^Z is $\langle p_T^Z \rangle = 5.4 \pm 1.0$ GeV/c.

14. THE WIDTH OF THE Z^0

In order to extract an estimate of the Z^0 width, Γ_Z, from the 13 events used to determine M_Z, we first note that the r.m.s. deviation of the mass values from the value of M_Z given by Eq. (12) is 3.58 GeV/c^2, which is very similar to the average of the measurement errors, $\sigma = 3.42$ GeV/c^2. Under these circumstances, and given the small statistical sample available, the determination of Γ_Z depends critically on a precise knowledge of the experimental mass resolution function.

For this reason we have carried out Monte Carlo studies using a large number of event samples, each consisting of 13 events, and created from Breit-Wigner distributions of varied Γ_Z values. The production and detection conditions have been included in detail. We have examined several estimators of Γ_Z. In all cases we find that the Monte Carlo distributions of the estimator results are biased, and considerable differences, D, between the mean and the most probable values result. Here, we compare two estimators. The first, ω, is a linear combination of several simple estimators constructed to minimize the difference D. The second is the maximum likelihood estimator, where D is large. In both cases we remove the bias as a function of Γ_Z, by reference to the mean of the Monte Carlo result.

From the real event sample, we obtain the estimate ω_{exp}. Defining the upper limit of Γ_Z as the value for which $\omega < \omega_{exp}$ in 90% of the Monte Carlo event samples, we then measure $\Gamma_Z < 3.3$ Gev/c^2 at the 90% confidence level. Using the maximum-likelihood estimator in the same way we measure $\Gamma_Z < 4.6$ GeV/c^2 at the 90 % confidence level. The difference between these two results reflects uncertainty resulting from the small statistical sample. The systematic error, resulting mainly from the uncertainty in the energy measurement error, is small.

Within the context of the Standard Model, the value of Γ_Z is related to the number of fermion doublets for which the decay $Z^0 \rightarrow f\bar{f}$ is kinematically allowed. In the case for which any additional W- and Z^0-decay products result from new fermion doublets in which only the neutrino is significantly less massive than $M_Z/2$, then

$$\Gamma_Z(\text{meas}) = \Gamma_Z(\text{three fermion families}) + 0.177\,\Delta n_\nu \qquad (14)$$

where Γ_Z is in units of GeV/c^2, and Δn_ν is the number of additional neutrino species.

Since Γ_W is independent of Δn_ν in this context if the associated charged lepton mass exceeds M_W, an independent estimate of Γ_Z can be obtained by measuring the ratio $R = \sigma_Z^e/\sigma_W^e$. In this case the error on R is dominated by statistics, because the value of the total integrated luminosity cancels out. From the observed numbers of $W \rightarrow e\nu$ and $Z^0 \rightarrow e^+e^-$ decays, and the corresponding detection efficiencies, we measure $R = 0.136^{+0.041}_{-0.033}$ averaged over data of $\sqrt{s} = 546$ GeV and $\sqrt{s} = 630$ GeV. QCD estimates of the ratio between the Z^0 and W production cross-sections [11] provide a relationship between R and the ratio Γ_W/Γ_Z :

$$\Gamma_W/\Gamma_Z = (8.9 \pm 0.9)\,R, \qquad (15)$$

where the error reflects the uncertainty of the QCD calculation [11] as well as the uncertainties of the values used for the partial widths. To calculate the partial widths we have used the measured M_W and M_Z values together with their errors.

Using the Standard Model value, Γ_W = 2.65 GeV/c² (which corresponds to the measured mass M_W = 81.2 GeV/c² and to a t-quark mass m_t = 40 GeV/c²), we find

$$\Gamma_Z = 2.19^{+0.7}_{-0.5}(\text{stat.}) \pm 0.22\ (\text{syst.})\ \text{GeV/c}^2 \qquad (16)$$

in good agreement with the Standard Model prediction of Γ_Z = 2.72 GeV/c² for M_Z = 92.5 GeV/c², assuming three fermion families and m_t = 40 GeV/c². We evaluate an upper limit for Δn_ν at the 90% confidence level from the lower limit R > 0.094, which gives Γ_Z < 3.17 ± 0.31 GeV/c². We obtain Δn_ν < 2.6 ± 1.7 (the errors reflect the uncertainties of Eq. 15).

The quoted limit on the additional number of neutrinos is valid subject to very specific conditions noted above. In most models for which an increase in Γ_Z is expected (for example the decay of Z^0 into super-symmetric particles) the Standard Model prediction for Γ_W is also affected.

15. $Z^0 \to ee\gamma$ AND THE SEARCH FOR $W \to e^*\nu$

Among the eight Z^0 events that were recorded in the 1983 data, we observed one event of the type $Z^0 \to ee\gamma$ [2,3,22]. The event contained a 24 GeV photon separated in space by 31° from an electron of 11 GeV. We can exclude external bremsstrahlung from the electron as it passed through the walls of the vacuum chamber or tracking system, because of its large e-γ opening angle. The process of internal bremsstrahlung can, however, produce such event topologies. We estimate that the probability of observing this eeγ configuration or a less likely configuration, in the sample of eight Z^0 events, is ~10% [3]. Since no similar events have been observed in the 1984 data, we conclude that the probability of the internal bremsstrahlung hypothesis has increased to 19%.

It should be noted that about 75% of the electrons produced from the decay of the Z^0 are detected in the central region of the UA2 detector. The absence of a magnetic field in this region

implies that both the electron and photon can be unambiguously identified only if they produce two distinct clusters in the calorimeter. This corresponds to a requirement that the electron and photon are separated by at least one cell at the calorimeter impact (in practice 20°-30°). If the electron and photon are seperated by less than ~50 mrads, the resulting signature is identical to that of an electron of energy $E = E_e + E_\gamma$, while for intermediate electron-photon separations the electron analysis criteria will not be satisfied.

Although the internal bremsstrahlung hypothesis is at present the most likely explanation of the eeγ event, many other interpretations have been suggested. One interpretation is the decay $Z^0 \to e^* e$ where e^* is an excited electron decaying into an e-γ pair [23]. The masses of the two e-γ combinations are 9.1 ± 0.3 GeV/c^2 and 74.7 ± 1.8 GeV/c^2. Excited electrons of the smaller mass have been excluded by searches at e^+e^- storage rings [24], while those of the larger mass have not. Presumably, such states would also couple to the W. We have therefore searched for the decay sequence $W \to e^* \nu \to e\gamma\nu$ [25]. The neutrino, in this case, can be either a conventional ν_e or an excited state (assumed to be much less massive than the e^*).

The search uses the sample of 2436 events that is described in Section 3. Each event in the sample contains at least one electron candidate having $E_T > 11$ GeV. We require that each event contains in addition at least one photon candidate, with $E_T > 11$ GeV and with an associated conversion in the preshower detector. A photon candidate is defined as an energy cluster in either the central or forward calorimeters subject to the following criteria:

i. the cluster is required to have small lateral extent and small hadronic leakage (see Section 3),

ii. no reconstructed track should point to the cluster,

iii. each candidate is required to have an associated signal in the preshower counter consistent with a photon conversion, and

iv. the shower development in the calorimeters should be consistent with that of a photon having a trajectory determined by the event vertex and the preshower signal.

Of the 2436 events in the sample, only the $Z^0 \rightarrow e^+e^-\gamma$ event contains a photon candidate. No candidate for the decay $W \rightarrow e\nu\gamma$ is observed. A total of 0.2 ± 0.1 events are expected from internal bremsstrahlung.

The interpretation of this result requires a Monte Carlo simulation of the process $p\bar{p} \rightarrow W \rightarrow e^*\nu \rightarrow e\gamma\nu$ in the detector. It is necessary to make some assumption about the coupling of an excited state to the W boson. We consider two possibilities. The first, favoured by many authors [23], is that the W couples to the transition magnetic moment of the e^*-ν current. The appropriate part of the effective Lagrangian can be written as

$$\mathcal{L} = (g/\sqrt{2})(\lambda_{mag}/M^*)W_\alpha^- \bar{e}^* \sigma^{\alpha\beta} q_\beta \nu_L + \text{h.c.} \qquad (17)$$

where g is the SU(2) coupling constant, λ_{mag} is a factor representing the coupling strength ($0 \leq \lambda_{mag} \leq 1$), M^* is the mass of the excited electron, and q is the 4-momentum of the W field. The second possibility is that the W couples to a standard V-A current. The effective Lagrangian can be written as

$$\mathcal{L} = (g/\sqrt{2})\lambda_{V\text{-}A} W_\alpha^- \bar{e}^* \gamma^\alpha \nu_L + \text{h.c.} \qquad (18)$$

where $\lambda_{V\text{-}A}$ is a factor representing the coupling strength ($0 \leq \lambda_{V\text{-}A} \leq 1$).

The Monte Carlo simulation is used to calculate the ratio of the accepted cross-section for the process $p\bar{p} \rightarrow W \rightarrow e^*\nu \rightarrow e\gamma\nu$ to the total cross-section for the process $p\bar{p} \rightarrow W \rightarrow e\nu$. Using this ratio, the measured W cross-sections (see Section 6), the electron efficiency (see Section 3), and the photon conversion efficiency of the preshower counter (approximately 70%), the number of expected events is calculated for various choices of M^* and λ_{mag} or $\lambda_{V\text{-}A}$. The results of these calculations are shown in Fig. 20 for both choices of coupling. They are represented as 90% confidence regions in λ-M^*

space for which the existence of excited electrons is excluded. The existence of a 75 GeV/c^2 excited electron is just excluded provided that it couples to the W with the full Standard Model coupling strength.

16. COMPARISON WITH THE SU(2) ⊗ U(1) MODEL

If we ignore the fermion and Higgs scalar masses, and the elements of the Kobayashi-Maskawa matrix [26], the minimal Standard Model is characterised by three parameters, which can be taken to be α (the fine structure constant), and the IVB masses M_W, M_Z. In order to compare our measurements with the predictions of the Standard Model, we must use suitably renormalised and radiatively corrected theoretical quantities [27]. We shall use the definition where [28]

$$\sin^2\theta_w = 1 - (M_W/M_Z)^2 \tag{19}$$

which leads to the following predictions for the IVB masses:

$$M_W{}^2 = A^2/[(1-\Delta r)\sin^2\theta_w] \tag{20}$$

$$M_Z{}^2 = 4A^2/[(1-\Delta r)\sin^2 2\theta_w] \tag{20'}$$

where $A = (\pi\alpha/\sqrt{2}G_F)^{1/2} = (37.2810 \pm 0.0003)$ GeV/c^2 using the measured values of α and G_F [9]. In the above equations, the value Δr reflects the effect of one-loop radiative corrections on the IVB masses and has been computed to be [28]

$$\Delta r = 0.0696 \pm 0.0020 \tag{21}$$

for $m_t = 36$ GeV/c^2 and assuming that the mass of the Higgs boson, M_H, is equal to M_Z. Although the quoted theoretical error in Eq. (21) is quite small, it has been pointed out [28,29] that Δr can be significantly decreased in the case of a very heavy t-quark ($\Delta r \approx 0$ for $m_t = 240$ GeV/c^2), or if a new fermion family exists with a large mass splitting between the two members of an SU(2) doublet.

Using Eqs. (20), (20′) and (21), we can extract two values of $\sin^2\theta_W$ from our measured values of M_W and M_Z. We then combine them to obtain our best estimate of $\sin^2\theta_W$:

$$\sin^2\theta_W = 0.226 \pm 0.005(\text{stat.}) \pm 0.008(\text{syst.}). \quad (22)$$

By using Eq. (19) it is possible to measure $\sin^2\theta_W$ with no systematic error from the uncertainty on the mass scale. We recall, however, that there is a ± 0.5 GeV/c^2 systematic uncertainty on the value of M_W which is not related to the energy calibration of the calorimeter (see Section 7). By taking this uncertainty into account we obtain

$$\sin^2\theta_W = 0.229 \pm 0.030(\text{stat.}) \pm 0.008(\text{syst.}), \quad (23)$$

which represents a much less precise measurement than the result of the method described previously.

Both the above results are in agreement with the value

$$\sin^2\theta_W = 0.220 \pm 0.008 \quad (24)$$

compiled from low energy data [30] together with recent results of the CDHS [31] and CCCFRR [32] experiments, after radiative corrections have been applied to these data. Very recent and accurate data from the CDHS [33] and CHARM [34] experiments do not significantly alter the average value of (24).

In the above discussion we have implicitly assumed the ρ parameter, defined as [35]

$$\rho = M_W^2/(M_Z^2 \cos^2\theta_W) \quad (25)$$

to be $\rho = 1$, which follows directly from the definition of $\sin^2\theta_W$ given by Eq. (19). However, by combining Eqs. (20) and (25) we obtain

$$\rho = M_W^2/[M_Z^2 (1 - B^2/M_W^2)] \quad (26)$$

where $B^2 = A^2/(1-\Delta r)$. In our data this is the only measurable quantity which is sensitive to the Higgs sector (more precisely, it depends on the isospin structure of the Higgs fields, but only very weakly on their masses). From Eq. (26) we obtain

$$\rho = 0.996 \pm 0.033(\text{stat.}) \pm 0.009(\text{syst.}), \tag{27}$$

in good agreement with the value $\rho = 1.02 \pm 0.02$ from low energy data (see the compilations of [28] and [36]), and with the minimal Standard Model.

Finally, we evaluate the sensitivity of our measurements to the radiative corrections expressed in terms of the quantity Δr. Using only our measurements, and eliminating $\sin^2\theta_W$ from Eqs. (20) and (20′), we obtain

$$\Delta r = 0.08 \pm 0.10(\text{stat.}) \pm 0.03(\text{syst.}). \tag{28}$$

If, on the other hand, we use the average value of $\sin^2\theta_W$ from low energy data (see Eq. 24), and combine the values of Δr obtained from Eqs. (20) and (20′), we obtain

$$\Delta r = 0.05 \pm 0.03(\text{stat.}) \pm 0.03(\text{syst.}). \tag{29}$$

Within the present statistical and systematic errors, we cannot demonstrate the existence of radiative corrections in the Standard Model, even if we include the results of low energy experiments. This conclusion is summarised in Fig. 21, which shows the 68% confidence level contours in the plot of $M_Z - M_W$ versus M_Z from our measurements, compared to the Standard Model predictions ($\rho = 1$) with and without radiative corrections. Also shown in Fig. 21 are the ranges of $\sin^2\theta_W$ and ρ allowed by the low energy measurements.

17. SUMMARY.

In the previous Sections, we have described data so far collected for the processes

$$\bar{p} + p \rightarrow W^{\pm} + \text{anything}$$

$$\rightarrow e^{\pm} + \nu(\bar{\nu}) + \text{anything, and}$$

$$\bar{p} + p \rightarrow Z^0 + \text{anything}$$

$$\rightarrow e^+ + e^- + \text{anything}$$

We have measured the cross-sections for these processes at $\sqrt{s} = 546$ GeV and $\sqrt{s} = 630$ GeV to be:

$$\sigma_W{}^e(546 \text{ GeV}) = 0.50 \pm 0.09 \text{ (stat.)} \pm 0.05 \text{ (syst.) nb}$$

$$\sigma_W{}^e(630 \text{ GeV}) = 0.53 \pm 0.06 \text{ (stat.)} \pm 0.05 \text{ (syst.) nb}$$

$$\sigma_Z{}^e(546 \text{ GeV}) = 110 \pm 39 \text{ (stat.)} \pm 9 \text{ (syst.) pb}$$

$$\sigma_Z{}^e(630 \text{ GeV}) = 52 \pm 19 \text{ (stat.)} \pm 4 \text{ (syst.) pb}$$

These results are in reasonable agreement with theoretical estimates [11], and with recent results from the UA1 Collaboration [10].

We have studied the associated production of W and Z^0 with high-p_T hadronic jets, and we have compared these data with expectations from higher-order QCD corrections to the basic W and Z^0 production sub-processes.

Updated measurements of the W and Z^0 masses and widths have been described. The new mass values are within errors consistent with those previously reported [3]:

$$M_W = 81.2 \pm 1.1 \text{ (stat.)} \pm 1.3 \text{ (syst.) GeV/c}^2$$

$$M_Z = 92.5 \pm 1.3 \text{ (stat.)} \pm 1.5 \text{ (syst.) GeV/c}^2.$$

Using the mass measurements alone, we have reported updated values of $\sin^2\theta_W$, taking the scheme used by Marciano and Sirlin [28]:

$$\sin^2\theta_W = 0.229 \pm 0.030(\text{stat.}) \pm 0.008(\text{syst.}).$$

Alternatively, using low-energy measurements of α and G_F, and one-loop radiative corrections as calculated in [28] with $m_t = 36$ GeV/c^2, we have measured:

$$\sin^2\theta_W = 0.226 \pm 0.005(\text{stat.}) \pm 0.008(\text{syst.}) \text{ for } \rho = 1, \text{ and}$$

$$\rho = 0.996 \pm 0.033(\text{stat.}) \pm 0.009(\text{syst.}).$$

These measurements are in good agreement with low-energy data [28,36], and with the predictions of the minimal Standard Model.

ACKNOWLEDGEMENTS

This experiment would have been impossible without the very successful operation of the CERN $\bar{p}p$ Collider whose staffs and coordinators we gratefully acknowledge for their collective effort.

We deeply thank the technical staffs of the institutes collaborating in UA2 for their important contributions to maintain and improve the performance of the detector.

We are grateful to the UA4 Collaboration for providing the signals from their small-angle scintillator arrays and to the UA5 Collaboration for the loan of scintillator hodoscopes.

Financial support from the Schweizerischer Nationalfonds zur Förderung der Wissenschaftlichen Forschung to the Bern group, from the Danish Natural Science Research Council to the Niels Bohr Institute group, from the Bundesministerium für Forschung und Technologie to the Heidelberg group, from the Institut National de Physique Nucléaire et de Physique des Particules to the Orsay group, from the Istituto Nazionale di Fisica Nucleare to the Pavia, Perugia and Pisa groups and from the Institut de Recherche Fondamentale (CEA) to the Saclay group are acknowledged.

TABLE 1.

Electron candidates of $p_T^e > 25$ GeV/c.

$\sqrt{s}$ (GeV)	546	630
Integrated luminosity (nb^{-1})	142.5 ± 11.5	310 ± 25
UA2 acceptance, ε	0.66 ± 0.01	0.65 ± 0.01
UA2 electron detection efficiency,		
η central	0.74 ± 0.04	0.74 ± 0.04
forward	0.79 ± 0.03	0.79 ± 0.03
ρ_{opp} efficiency	0.95 ± 0.02	0.93 ± 0.02
Number of electrons candidates :		
all ρ_{opp}	67	153
$\rho_{opp} < 0.2$	36	83
Background ($\rho_{opp} < 0.2$) :		
QCD	1.7 ± 0.5	4.1 ± 1.2
$W \to \tau\nu$	0.5 ± 0.1	1.2 ± 0.2
$Z^o \to e^+e^-$	1.1 ± 0.3	3.3 ± 1.0
Signal (electrons)	34.3 ± 6.0	78.9 ± 9.2
Signal ($W \to e\nu$)	32.7 ± 5.9	74.4 ± 9.0

Table II.

Systematic uncertainties on the measurement of M_W (GeV/c^2)

Source	Fit to the p_T^e spectrum	Fit to the M_T spectrum
$<p_T^W>$	± 0.6 GeV/c^2	–
ρ_{opp} cut	± 0.3 GeV/c^2	–
Γ_W†	± 0.2 GeV/c^2	± 0.2 GeV/c^2
p_T^ν measurement	–	± 0.3 GeV/c^2
Cell-to-cell calibration	± 0.2 GeV/c^2	± 0.3 GeV/c^2
Total of above	± 0.8 GeV/c^2	± 0.5 GeV/c^2
Absolute calibration	± 1.3 GeV/c^2	± 1.3 GeV/c^2

† Systematic uncertainty obtained by varying Γ_W by ± 0.5 GeV/c^2.

TABLE III

Z^o Event parameters

Event	Z1	Z2	Z3	Z4	Z5	Z6	Z7	Z8	Z9	Z10	Z11	Z12	Z13	Z14	Z15	Z16
Configuration	C-F	C-C	C-C	C-C	C-C	C-F	C-F eeγ	C-F	C-F	C-C	C-C	C-F	C-C	C-C	C-F	C-C
Mass (GeV/c^2)	94.1 ±2.1	93.7 ±2.7	86.4 ±2.0	92.5 ±3.3	86.5 ±2.1	95.7 ±3.5	90.4 ±3.8	90.2 ±2.1	100.1 ±2.5	90.8 ±4.1	90.2 ±3.0	91.7 ±2.6	97.5 ±5.9	79.8 ±5.7	92.2 ±2.3	94.3 ±2.9
p_T (GeV/c)	1.2	11.9	6.6	2.5	6.2	4.9	1.7	1.2	2.0	5.6	4.8	11.3	14.8	3.0	7.0	2.4
p_L (GeV/c)	-127.3	72.6	-41.7	-45.8	-1.9	-22.0	-54.0	-79.1	-25.2	0.5	-13.3	-47.6	-12.1	5.1	62.4	-32.7
n_{jets}		1								1		1				
E_T^{jets} (GeV)		6.8								10.7		7.3				
θ^o (e_1)	155.6	61.3	126.6	132.3	114.8	148.3	150.2	142.2	151.2	100.9	123.7	153.6	60.7	83.7	28.1	144.9
ϕ^o (e_1)	326.1	299.6	346.7	123.3	198.5	173.5	220.0	218.7	76.7	236.0	26.5	317.5	233.2	219.4	8.3	142.1
E (e_1) GeV	105.4 ±1.8	48.3 ±1.4	49.3 ±1.1	58.5 ±3.2	44.5 ±1.0	58.6 ±1.3	69.7 ±1.4	71.7 ±1.4	61.0 ±1.3	42.8 ±3.4	46.3 ±1.5	63.9 ±1.4	43.2 ±4.9	41.0 ±4.8	71.8 ±1.4	59.7 ±2.6
θ^o (e_2)	126.3	45.8	105.2	98.2	66.6	45.5	78.5	81.9	117.7	47.9	79.7	74.0	76.0	126.3	89.1	91.3	66.3
ϕ^o (e_2)	147.2	130.1	162.1	306.3	27.2	1.7	27.7	59.5	38.2	255.5	58.0	206.0	145.2	70.9	42.9	194.1	322.3
E (e_2) GeV	52.9 ±1.4	70.8 ±2.7	46.9 ±1.2	44.7 ±1.5	42.2 ±1.2	39.7 ±2.5	24.5 ±1.2 (γ)	11.1 ±.6	48.3 ±1.	42.2 ±1.2	48.2 ±1.2	45.0 ±2.1	40.0 ±1.5	56.1 ±1.4	39.0 ±2.9	39.8 ±1.2	40.1 ±1.1

REFERENCES

1. UA2 Collaboration. M. Banner et al., Phys. Lett. **122B** (1983) 476.

2. UA2 Collaboration. P. Bagnaia et al., Phys. Lett. **129B** (1983) 130.

3. UA2 Collaboration. P. Bagnaia et al., Z. Phys. C - Particles and Fields |24| (1984),1.

4. UA2 Collaboration. B. Mansoulié : The UA2 apparatus at the CERN $\bar{p}p$ Collider, Proc. of the 3rd Moriond Workshop on $\bar{p}p$ Physics (1983) p. 609 : éditions Frontières 1983.

5. UA2 Collaboration. A. Beer et al., Nucl. Inst. Meth. **224** (1984) 360.

6. UA4 Collaboration. M. Bozzo et al., Phys. Lett. **147B** (1984) 392.
   UA4 Collaboration. G. Sanguinetti : Proc. 3rd Moriond Workshop on $\bar{p}p$ Physics (1984) p. 25 : éditions Frontières 1983.

7. UA2 Collaboration. P. Bagnaia et al., Z. Phys. C - Particles and Fields |20|, (1983) 117.
   UA2 Collaboration. P. Bagnaia et al., Phys. Lett. **144B** (1984) 283.

8. S.D. Ellis, R. Kleiss and W.J. Stirling, Phys. Lett. **154B** (1985) 435.

9. Particle Data Group, Rev. Mod. Phys. **56** (1984) 1.

10. UA1 Collaboration. G. Arnison et al., W Production Properties at the CERN SPS Collider. Submitted to Phys. Lett. B.

11. G. Altarelli, R.K. Ellis, M. Greco and G. Martinelli, Nucl. Phys. **B246** (1984) 12.
    G. Altarelli, R.K. Ellis and G. Martinelli, Z. Phys. C - Particles and Fields **27** (1985) 617.

12. M. Glück et al., Z. Phys. C - Particles and Fields **13** (1982) 119.

13. UA1 Collaboration. G. Arnison et al., Phys. Lett. **129B** (1983) 273.

14. UA2 Collaboration. H. Hänni : Search for Monojet and Multijet events with large missing p_T in the UA2 experiment, preprint CERN-EP/85-87 (1985). To be published in Proc. of 5th. Topical Workshop on $p\bar{p}$ Collider Physics, St. Vincent, 1985.

15. UA1 Collaboration. G. Arnison et al., Phys. Lett. **139B** (1984) 115.

16. J.C. Collins and D.E. Soper : Nucl. Phys. **B193** (1981) 381 ; Nucl. Phys. **B194** (1982) 4445 ; Nucl. Phys. **B197** (1982) 446.

17. F. Halzen and W. Scott, Phys. Lett. **78B** (1978) 318 ;
B. Humpert and W.L. van Neervan, Phys. Lett. **93B** (1080) 456 ;
P. Aurenche and J. Lindfors, Nucl. Phys. **B185** (1981) 274 ;
P. Minkowski, Phys. Lett. **139B** (1984) 431 ;
See also Refs. 2-9 of reference [11b].

18. UA2 Collaboration. P. Bagnaia et al., Phys. Lett. **139B** (1984) 105.

19. UA2 Collaboration. H. Plothow-Besch : Associated Production of W's and Z's with Jets in UA2, preprint CERN-EP/85-86 (1985). To be published in Proc. of 5th. Topical Workshop on $p\bar{p}$ Collider Physics, St. Vincent, 1985.

20. UA2 Collaboration. J. A. Appel et al., Measurement of the $\sqrt{s}$ Dependence of Jet Production at the CERN $\bar{p}p$ Collider, CERN-EP/85-111 (1985) submitted to Phys. Lett. B.

21. S.D. Ellis, R. Kleiss and W.J. Stirling, Jet Activity in $W^{\pm}$, Z^0 Events - A Theoretical Analysis, CERN-TH.4185/85.

22. Similar events were also reported by the UA1 Collaboration. See
G. Arnison et al., Phys. Lett. **135B** (1984) 250.

23. K. Enqvist and J. Maalampi, Helsinki University preprint HU-TFT 83-46 ;
A. De Rujula, L. Maiani, and R. Petronzio, Phys. Lett. **140B**, 253 (1984);

N. Cabibbo, L. Maiani, and Y. Srivastava, University of Rome preprint n. 381, November 1983.

24. MARK J Collaboration. B. Adeva et al., Phys. Rev. Lett. **48** (1982) 967.

25. A candidate for the process $W \to e\gamma\nu$ was observed in the 1983 data (see ref. 1). It contained a collinear e-γ pair in the forward region of the detector. Since the mass of the pair is quite small, the observation is not relevant to this discussion.

26. M. Kobayashi and K. Maskawa, Prog. Theor. Phys. **49** (1973) 652.

27. A. Sirlin, Phys. Rev **D22** (1980) 971 ;
W. J. Marciano, Phys. Rev. **D20** (1979) 274 ;
M. Veltman, Phys. Lett. **91B** (1980) 95 ;
F. Antonelli et al., Phys. Lett. **91B** (1980) 90.

28. W. J. Marciano and A. Sirlin, Phys. Rev. **D29** (1984) 945.

29. M. Veltman, Nucl. Phys. **B123** (1977) 89 ;
Z. Hioki, Nucl. Phys. **B229** (1983) 284.

30. W. J. Marciano and A. Sirlin, Nucl. Phys. **B189** (1981) 442.
For a more recent review see J. Panman, CERN-EP/85-35 (1985).

31. CDHS Collaboration. H. Abramowicz et al., Z. Phys. **C28** (1985) 51.

32. CCFRR Collaboration. P.G. Reutens et al., Phys. Lett. **152B** (1985) 404.

33. CDHS Collaboration. A. Blondel, Contribution to the Europhysics Intl. Conf. on High Energy Physics, Bari, 1985.

34. CHARM Collaboration. F. Bergsma et al., A Precision Measurement of the Ratio of Neutrino induced Neutral-current and Charged-current Total Cross-sections, CERN-EP/85-113 (1985).

35. D. Ross and M. Veltman, Nucl. Phys. **B95** (1975) 135 ;

P. Q. Hung and J. J. Sakurai, Nucl. Phys. **B143** (1978) 81.

36. J. Kim et al., Rev. Mod. Phys. **53** (1980) 211.

For more recent reviews see:

P. Langacker, Proc. XXII Int. Conf. on High-Energy Physics, Leipzig (1984) pp 215-238;

A. Pullia, in Fifty Years of Weak Interaction Physics (1984) pp 333-415.

FIGURE CAPTIONS

1. Transverse momentum spectrum, dn/dp_T^e, of all electron candidates with $p_T^e > 11$ GeV/c for the 1982-1984 data samples. The electrons of the final $W^{\pm}$ sample (119 electrons) and Z^0 sample (21 electrons) are emphasized.

2. Transverse momentum spectrum of the highest-p_T electron candidate, for

   a. 1827 events satisfying $p_T^e > 11$ GeV/c and $\rho_{opp} > 0.2$. The background shape from a sample of π^0 events is superimposed, normalised in the range $p_T^e > 13$ GeV/c.

   b. 593 events satisfying $p_T^e > 11$ GeV/c and $\rho_{opp} \leq 0.2$. The expected background from QCD processes is superimposed (.....), together with expected contributions from decays $W \to \tau\nu$ (_ _ _) and $Z^0 \to e^+e^-$ with one electron escaping the acceptance (_.._..). The contribution of $W \to e\nu$ decays is shown (_._.), together with the total expectation from all processes (_____).

3. The distribution of p_T^e vs. p_T^ν for all events which contain an electron candidate having $p_T^e > 11$ GeV/c. The superimposed lines represent $p_T^\nu = p_T^e$. In a) all events are plotted, and in b) events with $\rho_{opp} \leq 0.2$ are shown.

4. The distribution of M_T for the 119 electron candidates having $p_T^e > 25$ GeV/c and $\rho_{opp} \leq 0.2$. Superimposed are the summed background contributions of Fig. 2b (.....), together with expectations of $W \to e\nu$ decay (_ _ _) and the sum of the curves (_____).

5. The distribution of p_T^{miss} for 63 events from the p_T^{miss} trigger in which an electromagnetic cluster exists satisfying $p_T > 30$ GeV/c and $p_T^{miss} > 30$ GeV/c. The superimposed curve represents the background from 2-jet events and from beam-gas background.

6. Plot of $\hat{p}^{-1}$ vs. E^{-1} for 28 $W \rightarrow e\nu$ candidates with $p_T^e > 20$ GeV detected in the forward regions. The quantity $\hat{p}$ is the product of the electron momentum as measured by magnetic deflection and the sign of the product $(q.\cos\theta_e)$ where $q = +1\ (-1)$ for $e^+(e^-)$.

7. The distribution of $|\cos\theta^*|$, where θ^* is the angle between the charged lepton and the direction of the incident protons in the $W^{\pm}$ rest frame, using the convention of Collins and Soper [16]. Corrections have been made for detector acceptance and resolution. The expected distribution $dn/d\cos\theta^* \propto 1+\cos^2\theta^*$, modified for the effect of higher-order QCD processes, is superimposed.

8. Distribution of the fractional longitudinal momentum, x, carried by interacting partons in the reaction $\bar{p}p \rightarrow W^{\pm}$ + anything, for a) data at $\sqrt{s} = 546$ GeV, and b) data at $\sqrt{s} = 630$ GeV. Superimposed Monte Carlo expectations take account of the detector acceptance and resolution.

9. Distribution of p_T^{ν} vs E_T^J, where E_T^J is the sum of all jet transverse energies ($\geq$ 5 GeV) in the event.

    a. a total of 807 events containing an electron of $p_T^e > 15$ GeV/c. The events in the region $p_T^{\nu} > 25$ GeV/c and $E_T^J > 30$ GeV, and also the Z^0 events, are emphasized.

    b. 3544 events from a background sample containing an energy cluster, of $E_T > 15$ GeV, compatible with the signature expected from a π^0.

10. The distribution of p_T^{ν} for 807 events satisfying $p_T^e > 15$ GeV/c. The expected background is superimposed.

11. The fraction $F_W(E_T^0)$ of $W \to e\nu$ decays associated with one or more jets having $E_T^J > E_T^0$, as a function of E_T^0. The number of events associated with bins of large E_T^J are shown on the figure.

    a. Combined 1983 and 1984 data sample. The superimposed curves are an evaluation of $F_{j_1 j_2}(E_T^0)$ from the data (− − −). The shaded region is the result of an evaluation of $F_W(E_T^0)$ from a QCD Monte Carlo [8], for α_s-values in the range 0.14 to 0.20.

    b. Data from 1983 and 1984 shown separately, with curves of $F_{j_1 j_2}(E_T^0)$ shown for each sample.

12. Distribution of p_T^W for 126 events (less 9.8 events background) from the 1983-84 data sample, satisfying $p_T^e > 15$ GeV/c and $p_T^\nu > 25$ GeV/c. The shaded region corresponds to 36 events (less background) having at least one jet of $E_T^J > 5$ GeV. The superimposed full curve is from Altarelli et al. [11], using D01 structure functions and calculated at $\sqrt{s} = 630$ GeV. The dotted curve is from Ellis et al. [8] at $\sqrt{s} = 630$ GeV.

13. Distribution of E_T^J, the transverse energy of the jet system J, for 36 $W \to e\nu$ decays with at least one associated jet, j, of $E_T^j > 5$ GeV. The expected distribution from QCD processes [8] is superimposed.

14. Distribution of M(WJ), the invariant mass of the W-jet(s) system, for 36 $W \to e\nu$ decays with at least one associated jet, j, of $E_T^j > 5$ GeV. The expected distribution from QCD processes [8] is superimposed. The distribution is not comparable to that of [18] because of different event selection criteria.

15. Distribution of $\tilde{E}_T$, the summed transverse energy of all particles detected in the range $|\eta| < 1$, for $W \rightarrow e\nu$ events (full line), and minimum-bias events (broken line). Only events with no associated jet activity are included. The minimum-bias curve is normalised to the area of the $W \rightarrow e\nu$ histogram.

16. Distribution of N_{ch}, the associated charged particle multiplicity, in $W \rightarrow e\nu$ decays with no associated jet (full line), and minimum-bias events (broken line). The minimum-bias curve is normalised to the area of the $W \rightarrow e\nu$ histogram.

17. The invariant mass distribution, M_{ee}, plotted for $M_{ee} > 20$ GeV/c^2 :

    a. 1154 events containing at least two clusters of $E_T > 5$ GeV and passing all calorimeter cuts of the electron analysis,

    b. a subsample of 54 events for which at least one clusters passes all electron identification criteria.

In each case, the expected background from 2-jet processes is superimposed.

18. For 16 events compatible with the decay $Z^0 \rightarrow e^+e^- (\gamma)$:

    a. the invariant mass distribution, $M_{ee(\gamma)}$, and

    b. individual mass values and their associated measurement uncertainties. Those marked (*) are not used in the mass determination [2,3], because of systematic uncertainties on the energy measurement of one electron.

19. Distribution of p_T^Z of 16 Z^0 events. The shaded region corresponds to 3 events having at least one associated jet of $E_T > 5$ GeV. The superimposed curve is from [11], calculated at $\sqrt{s} = 630$ GeV using DO1 structure functions as quoted in that reference.

20. 90% confidence regions in the $\lambda - M^*$ plane for which the existence of excited electrons of mass M^* is excluded. The parameter λ defines the strength of the coupling, as discussed in the text.

21. 68% confidence contours in the plot of $M_Z - M_W$ vs M_Z taking into account the statistical error only (1), and with statistical and systematic errors combined in quadrature (2). Curve a) is the Standard Model prediction for $\rho = 1$ with radiative corrections. Curve b) is the same prediction without radiative corrections. The band defined by curves a) and c) corresponds to the region allowed by the low energy result [28,36], $\rho = 1.02 \pm 0.02$. The curves corresponding to two different values of $\sin^2\theta_W$ define the region allowed by the world average of low energy results [30-32], $\sin^2\theta_W = 0.220 \pm 0.008$.

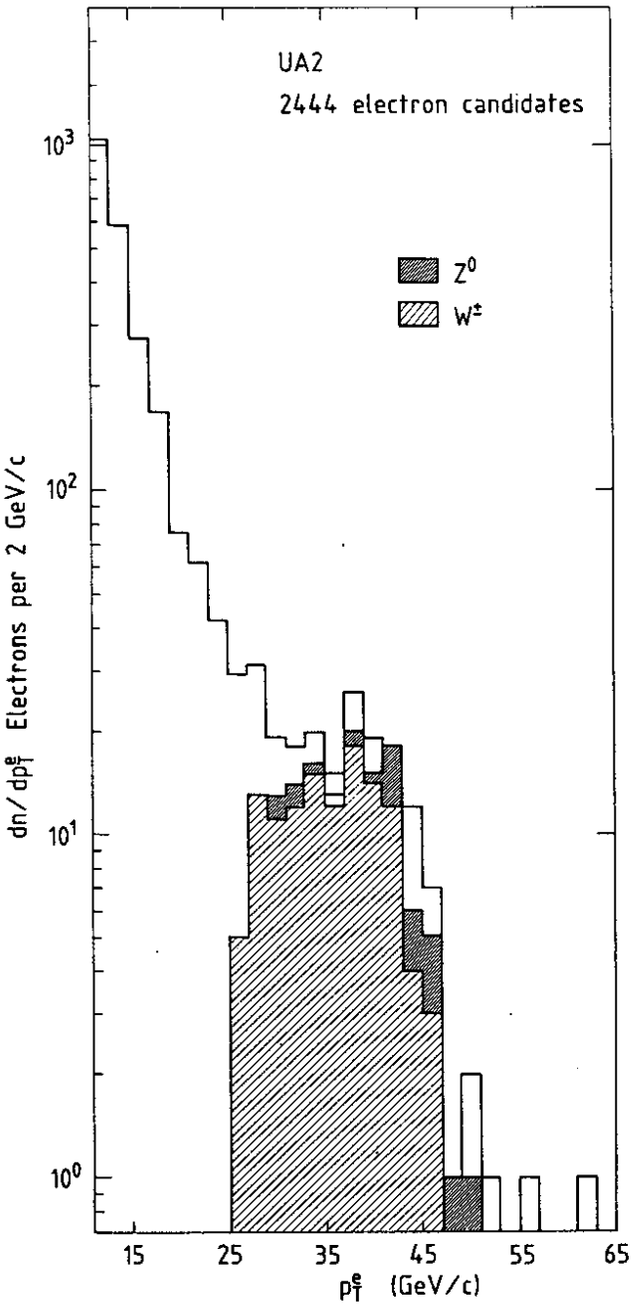
UA2
2444 electron candidates
Z^0
$W^{\pm}$
10^3
10^2
10^1
10^0
dn/dp_T^e Electrons per 2 GeV/c
15
25
35
45
55
65
p_T^e (GeV/c)

Fig. 1

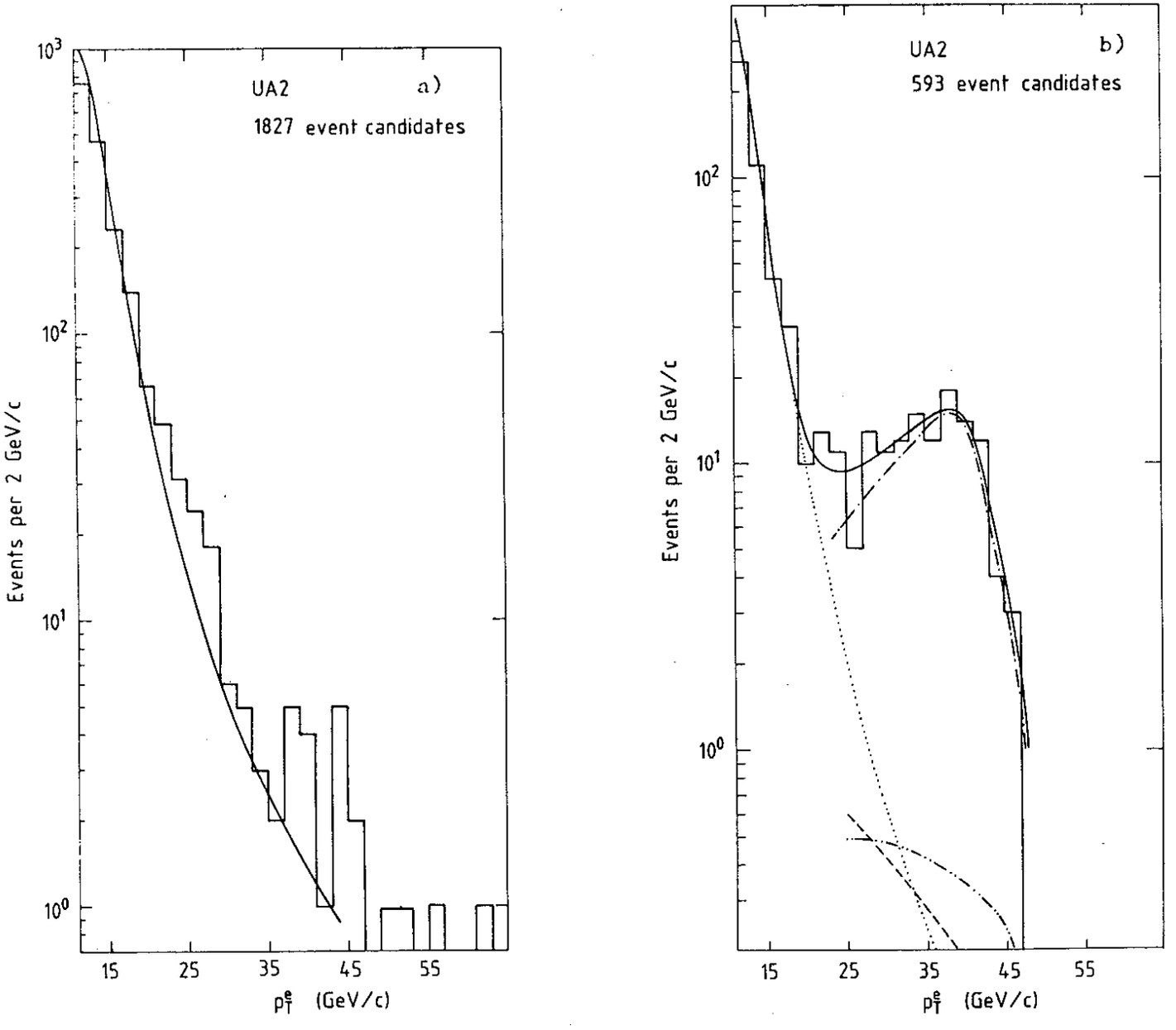
UA2
a)
1827 event candidates
Events per 2 GeV/c
10^3
10^2
10^1
10^0
15
25
35
45
55
p_T^e (GeV/c)
UA2
b)
593 event candidates
Events per 2 GeV/c
10^2
10^1
10^0
15
25
35
45
55
p_T^e (GeV/c)

Fig. 2

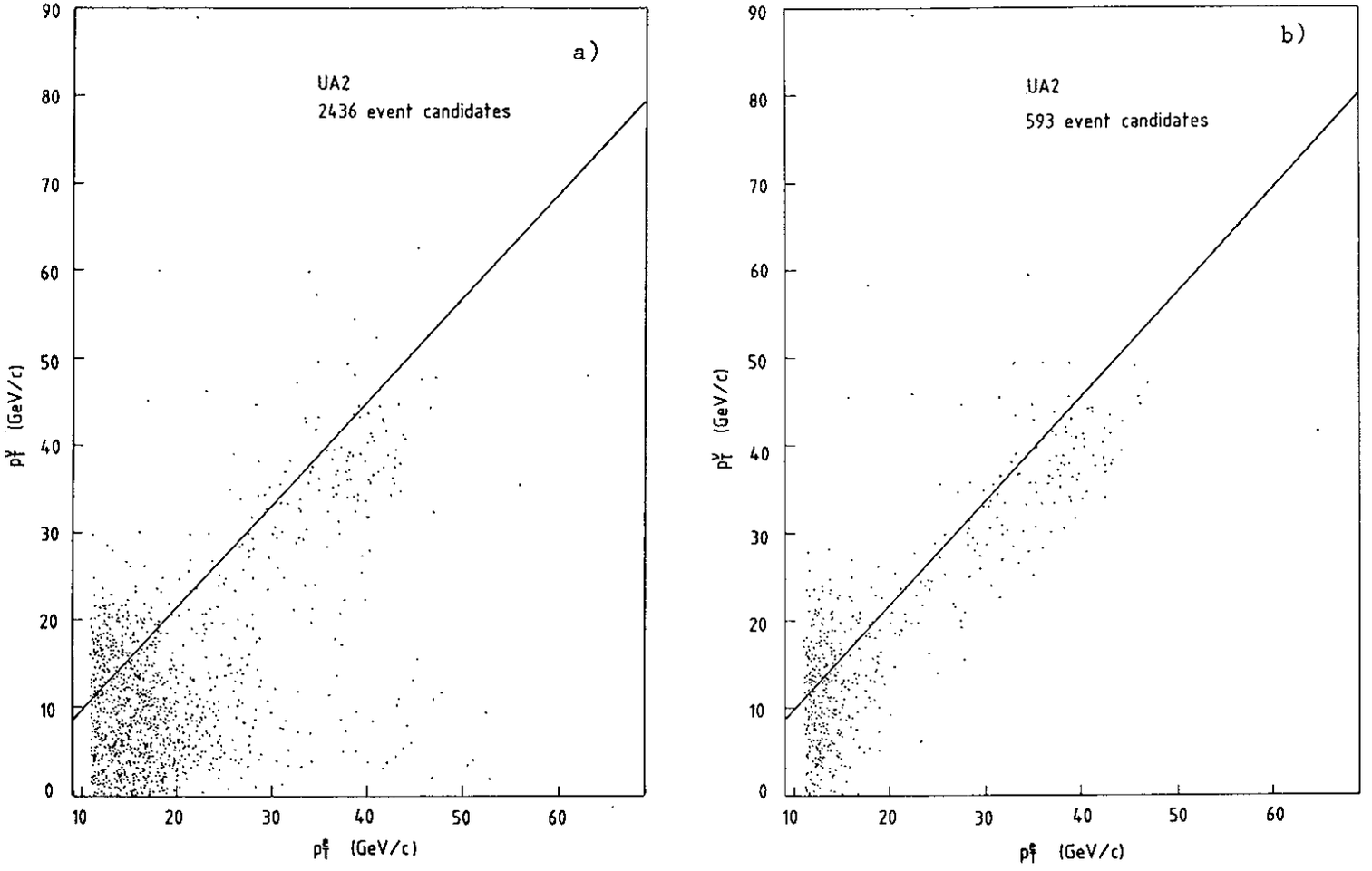
a)
UA2
2436 event candidates
b)
UA2
593 event candidates
p_T^ν (GeV/c)
p_T^e (GeV/c)
0
10
20
30
40
50
60
70
80
90

Fig, 3

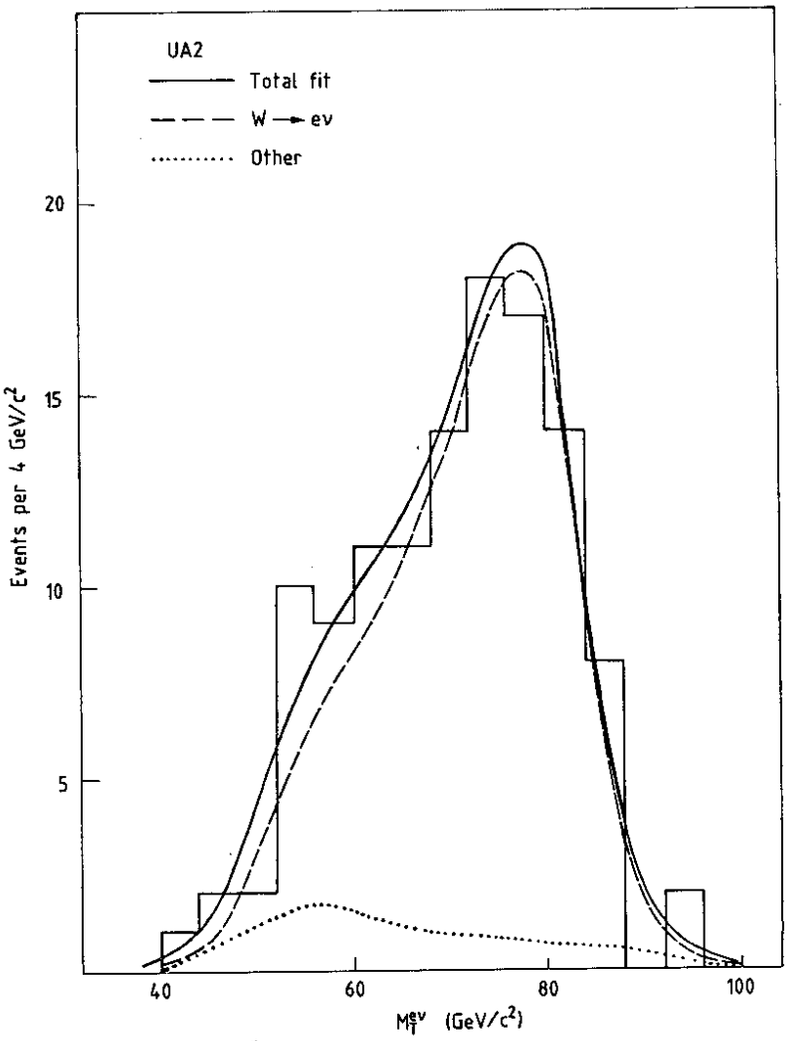
UA2
Total fit
W → eν
Other
Events per 4 GeV/c²
20
15
10
5
40
60
80
100
M_T^eν (GeV/c²)

Fig. 4

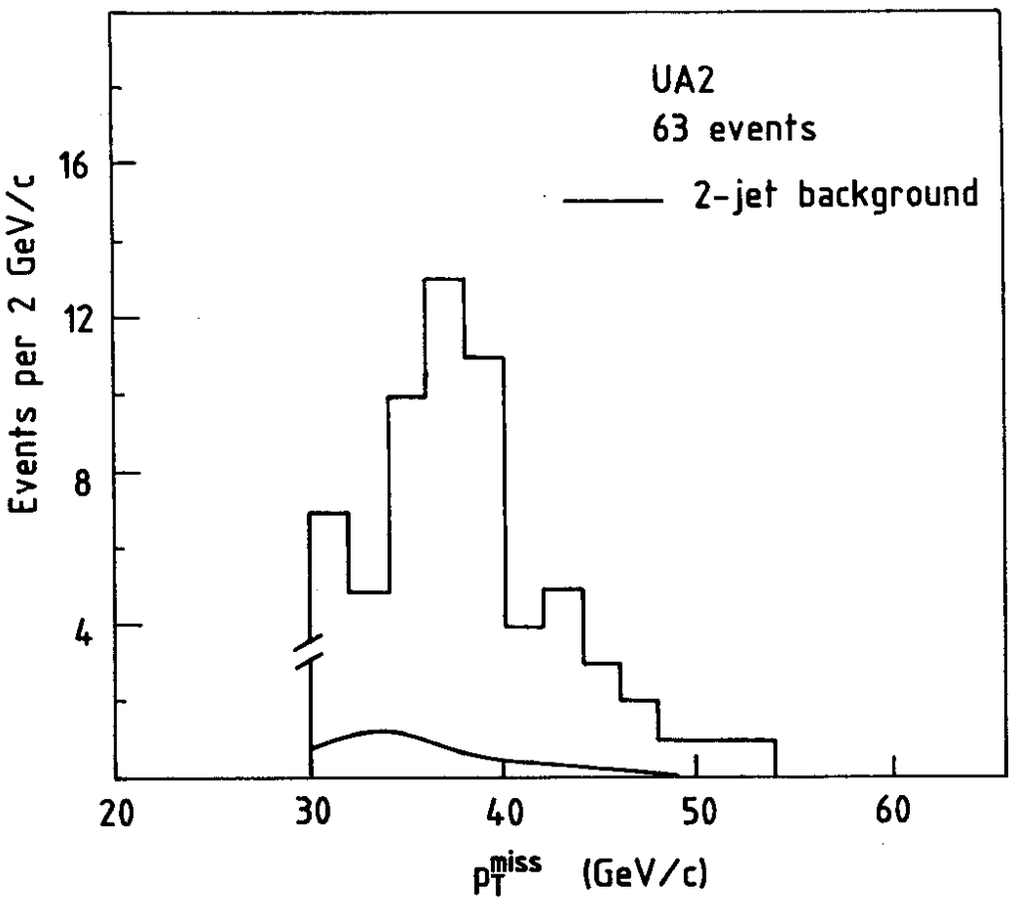
UA2
63 events
2-jet background
Events per 2 GeV/c
16
12
8
4
20
30
40
50
60
p_T^{miss} (GeV/c)

Fig. 5

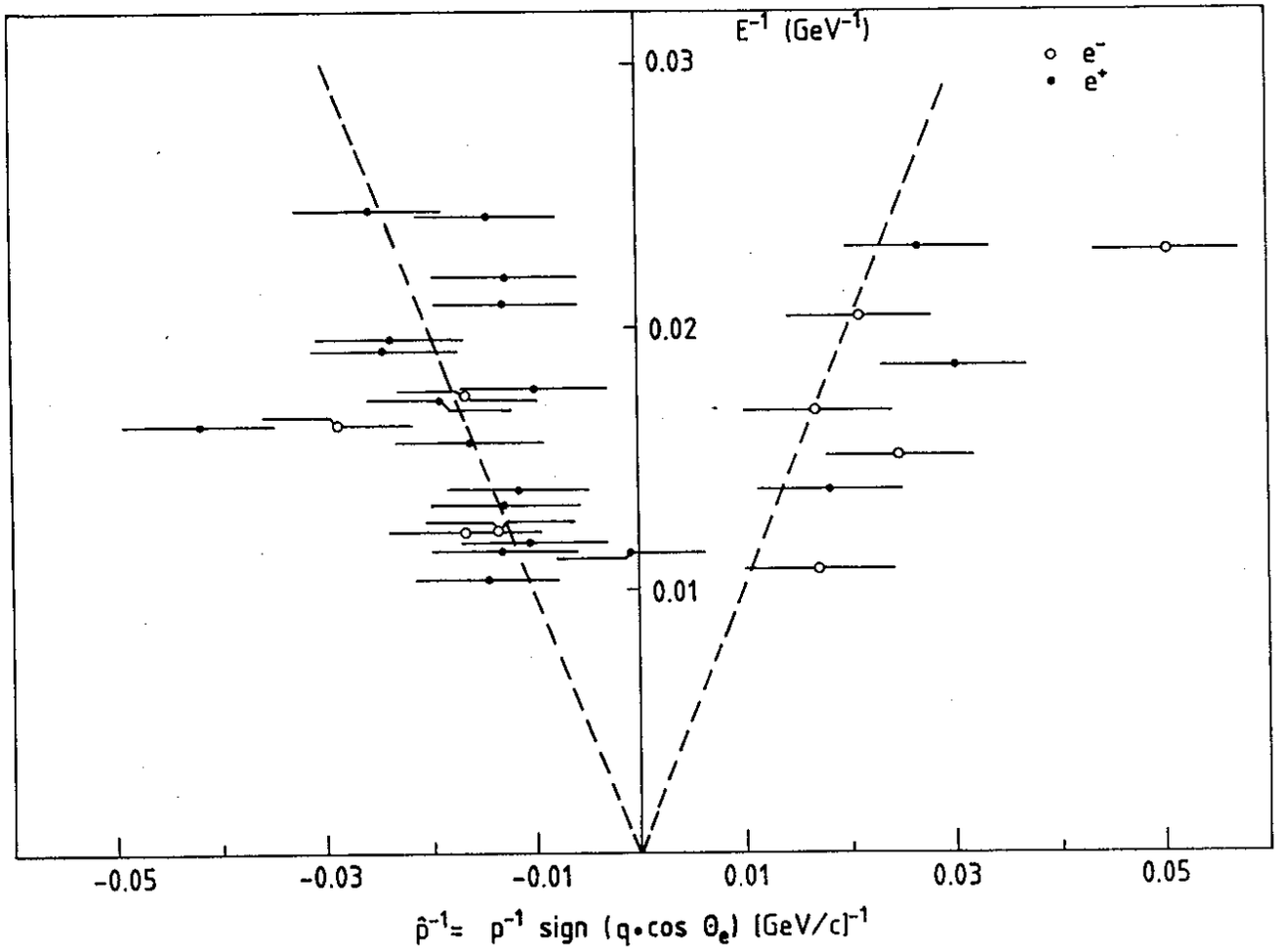
E^{-1} (GeV^{-1})
e^-
e^+
0.03
0.02
0.01
-0.05
-0.03
-0.01
0.01
0.03
0.05
$\hat{p}^{-1}$= p^{-1} sign ($q \cdot \cos \theta_e$) [GeV/c]$^{-1}$

Fig. 6

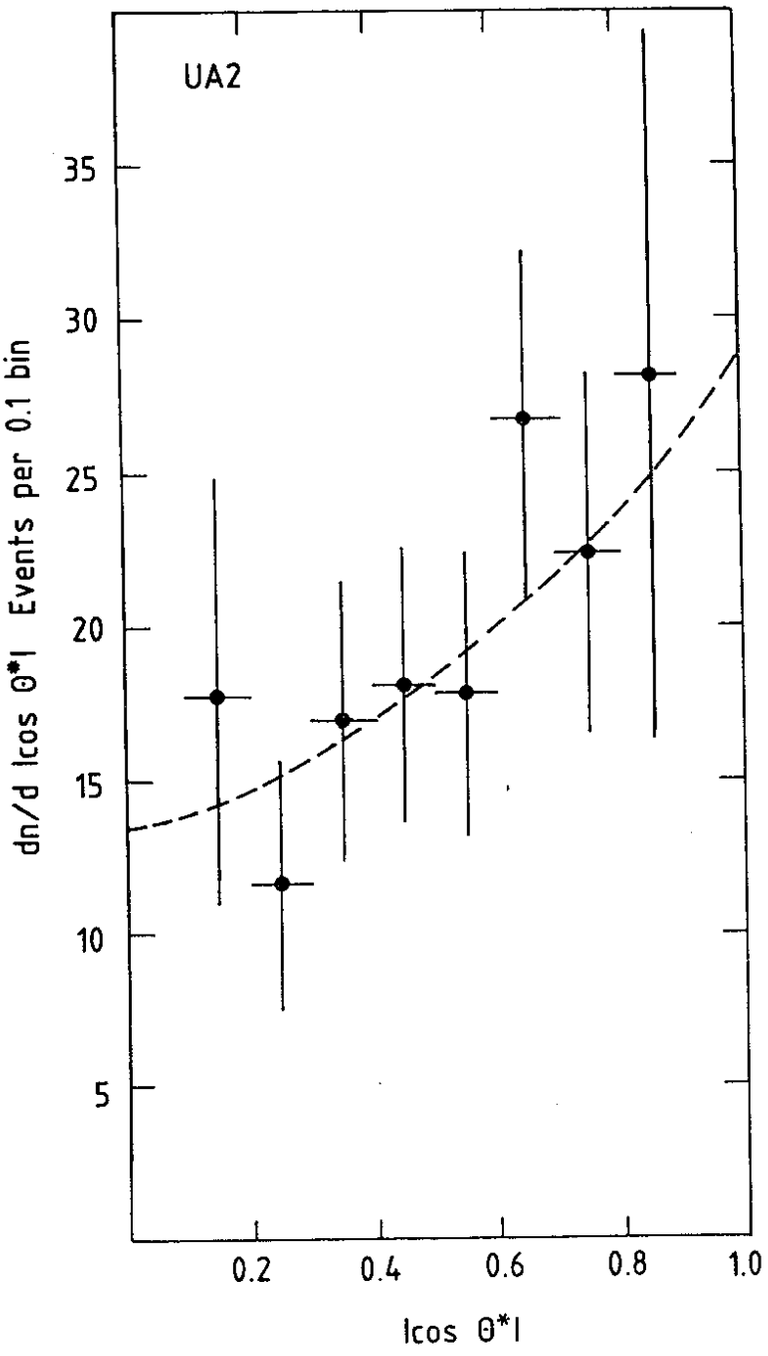
UA2
35
30
25
20
15
10
5
dn/d |cos θ*| Events per 0.1 bin
0.2
0.4
0.6
0.8
1.0
|cos θ*|

Fig. 7

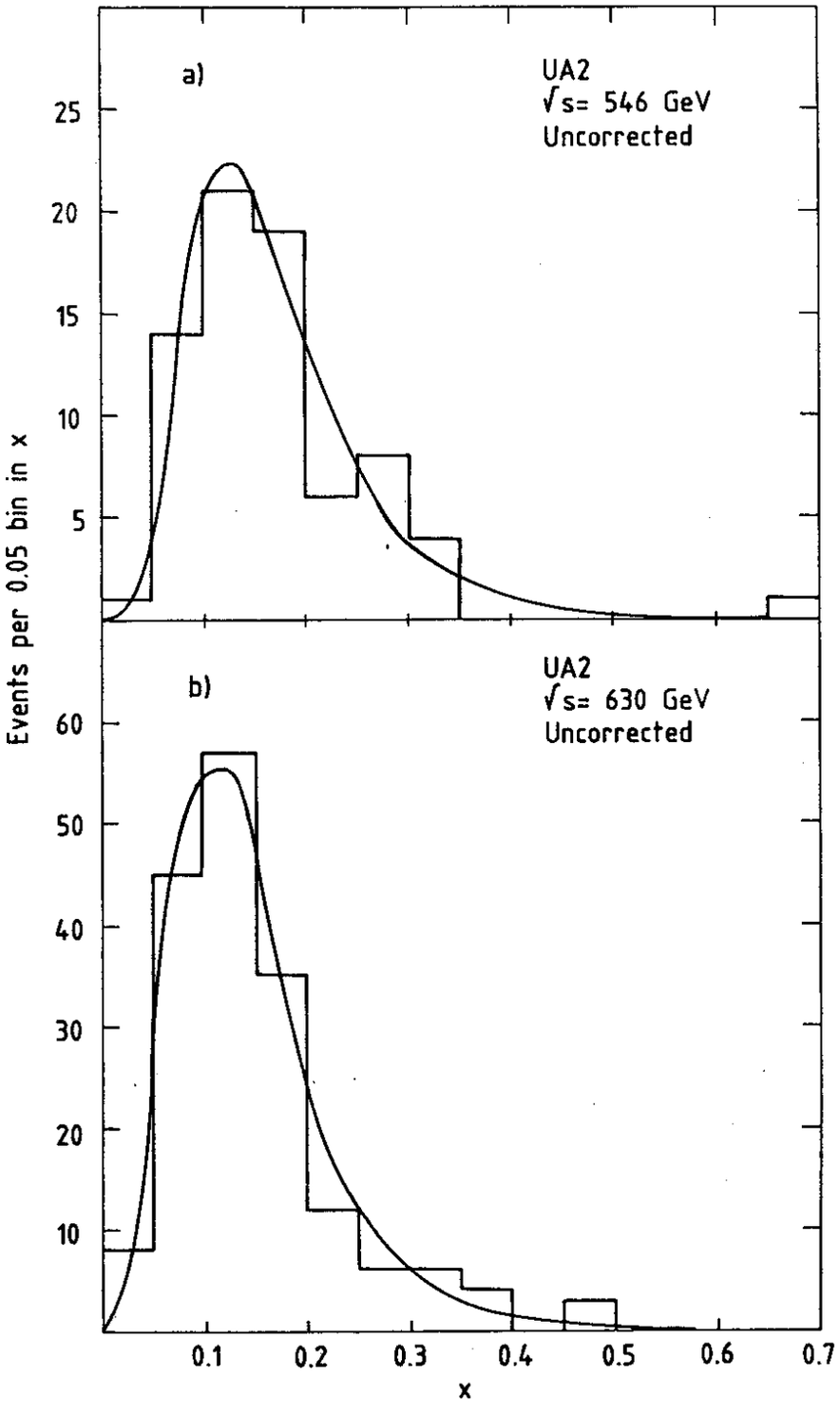
a)
UA2
√s= 546 GeV
Uncorrected
b)
UA2
√s= 630 GeV
Uncorrected
Events per 0.05 bin in x
x
25
20
15
10
5
60
50
40
30
20
10
0.1
0.2
0.3
0.4
0.5
0.6
0.7

Fig. 8

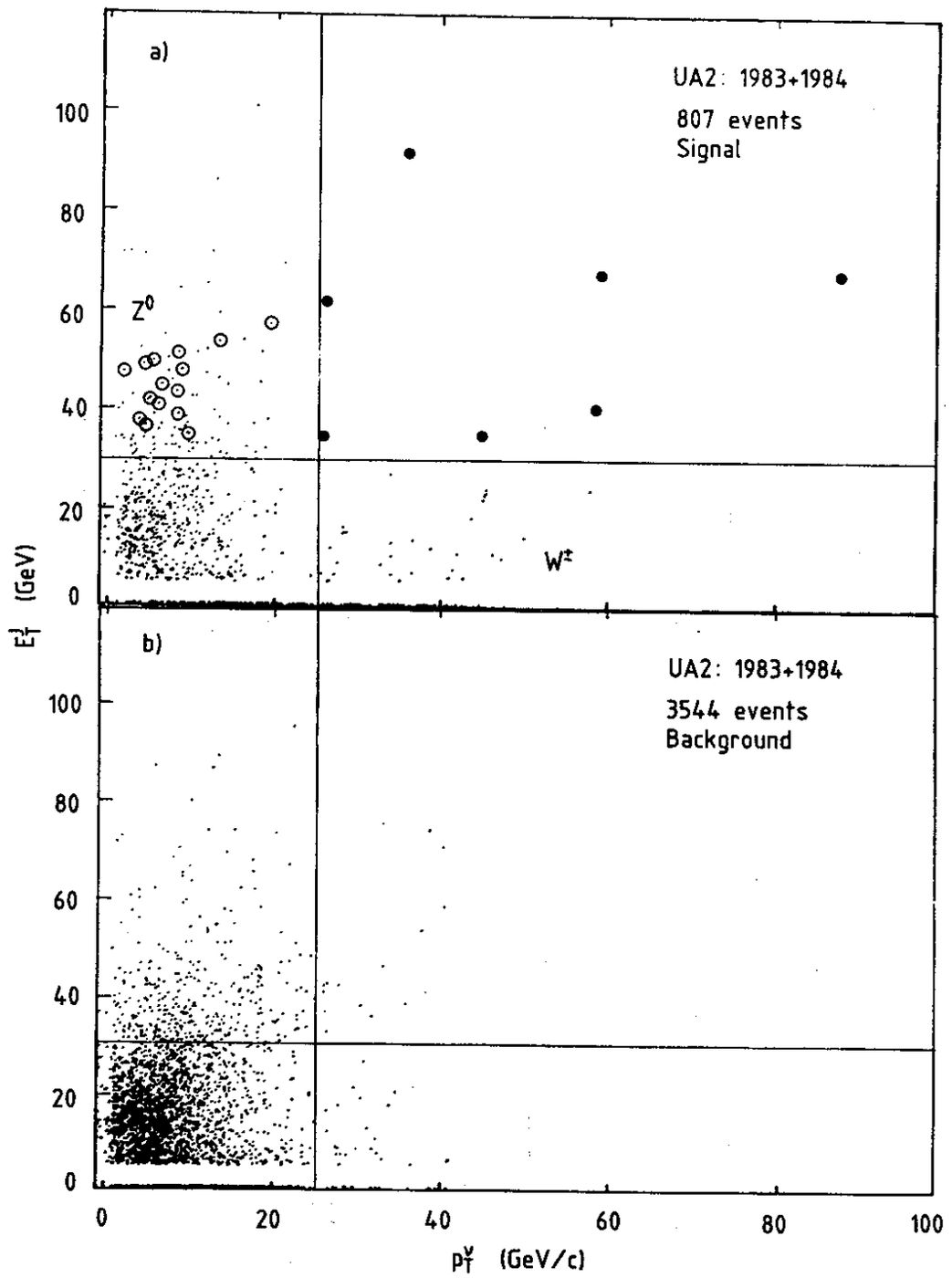
a)
UA2: 1983+1984
807 events
Signal
Z⁰
W±
b)
UA2: 1983+1984
3544 events
Background
E_T^l (GeV)
p_T^ν (GeV/c)
0
20
40
60
80
100

Fig. 9

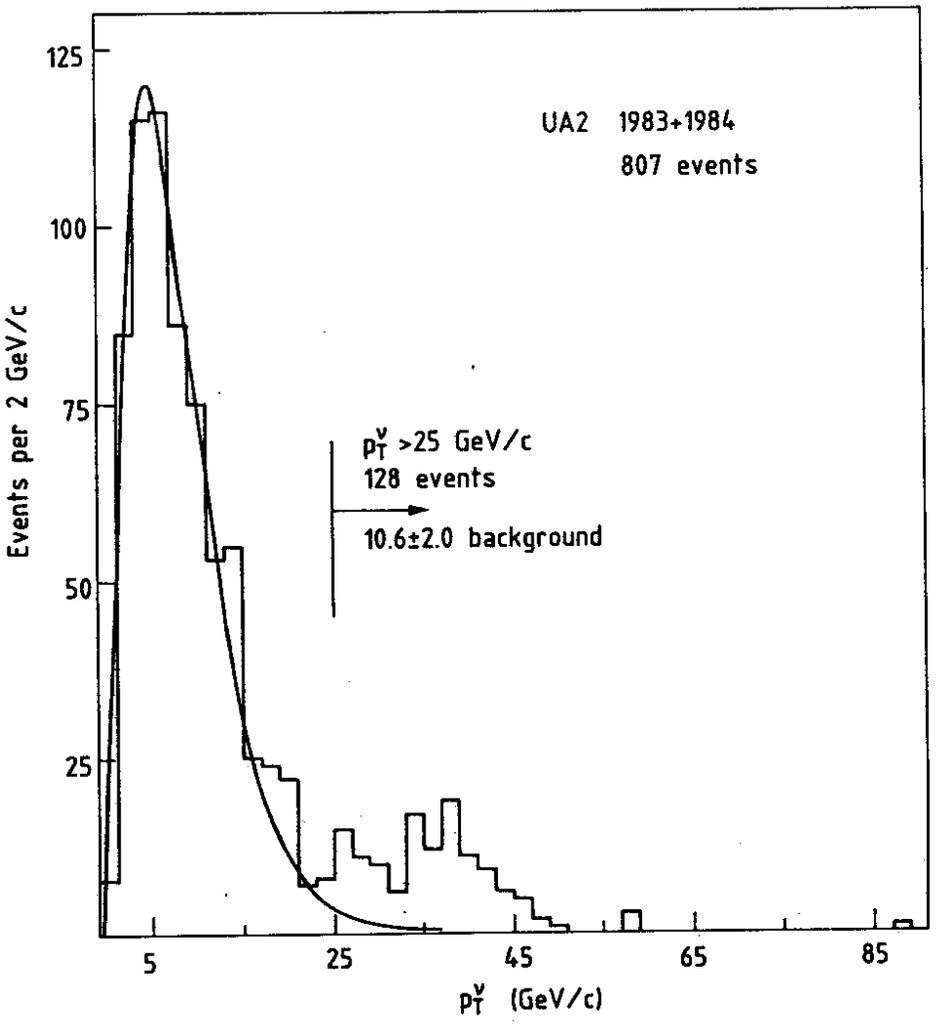
125
100
75
50
25
Events per 2 GeV/c
UA2 1983+1984
807 events
p_T^ν >25 GeV/c
128 events
10.6±2.0 background
5
25
45
65
85
p_T^ν (GeV/c)

Fig. 10

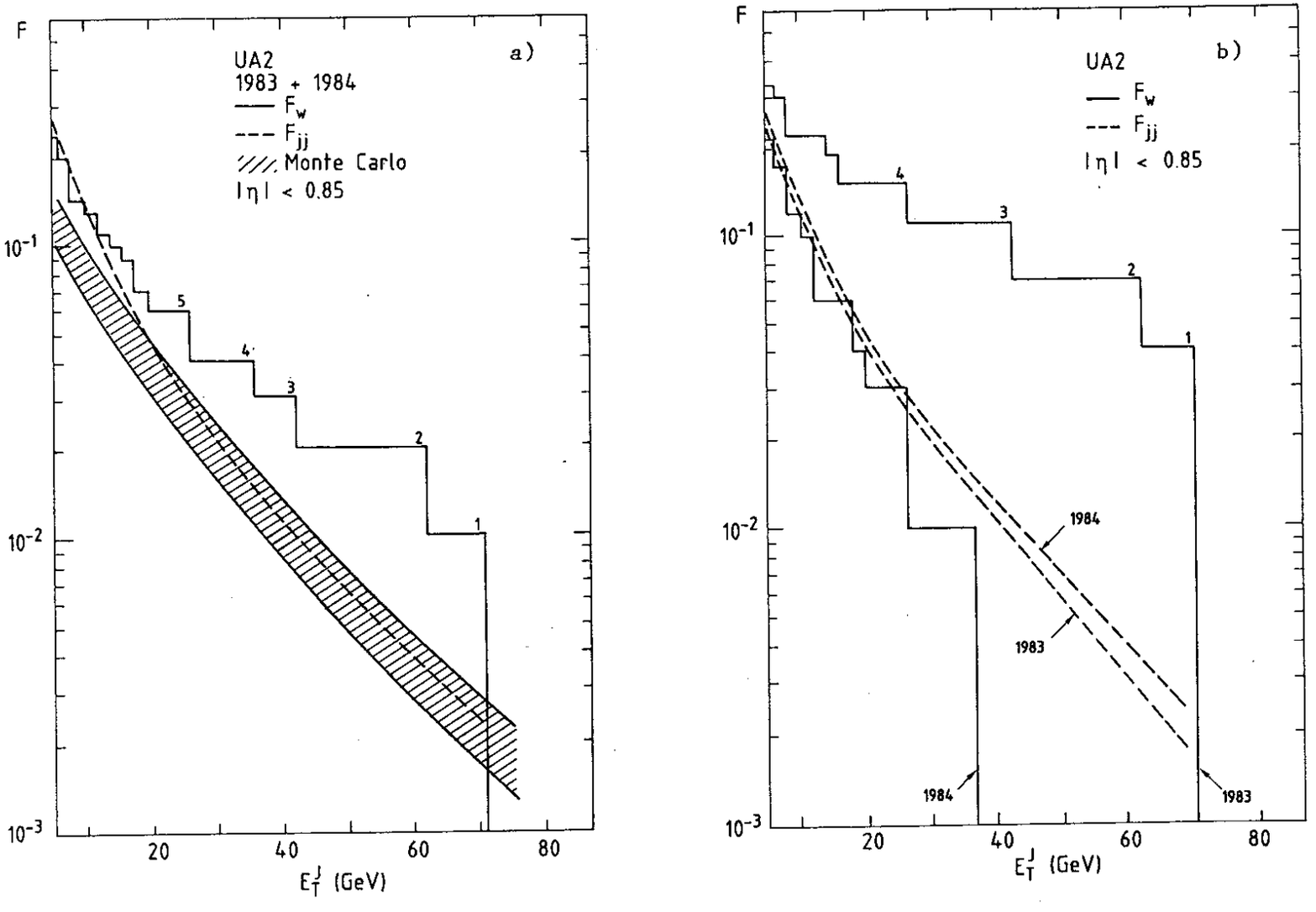
F
UA2
1983 + 1984
F_w
F_{jj}
Monte Carlo
$|\eta| < 0.85$
a)
b)
10^{-1}
10^{-2}
10^{-3}
20
40
60
80
E_T^J (GeV)
1
2
3
4
5
1984
1983

Fig. 11

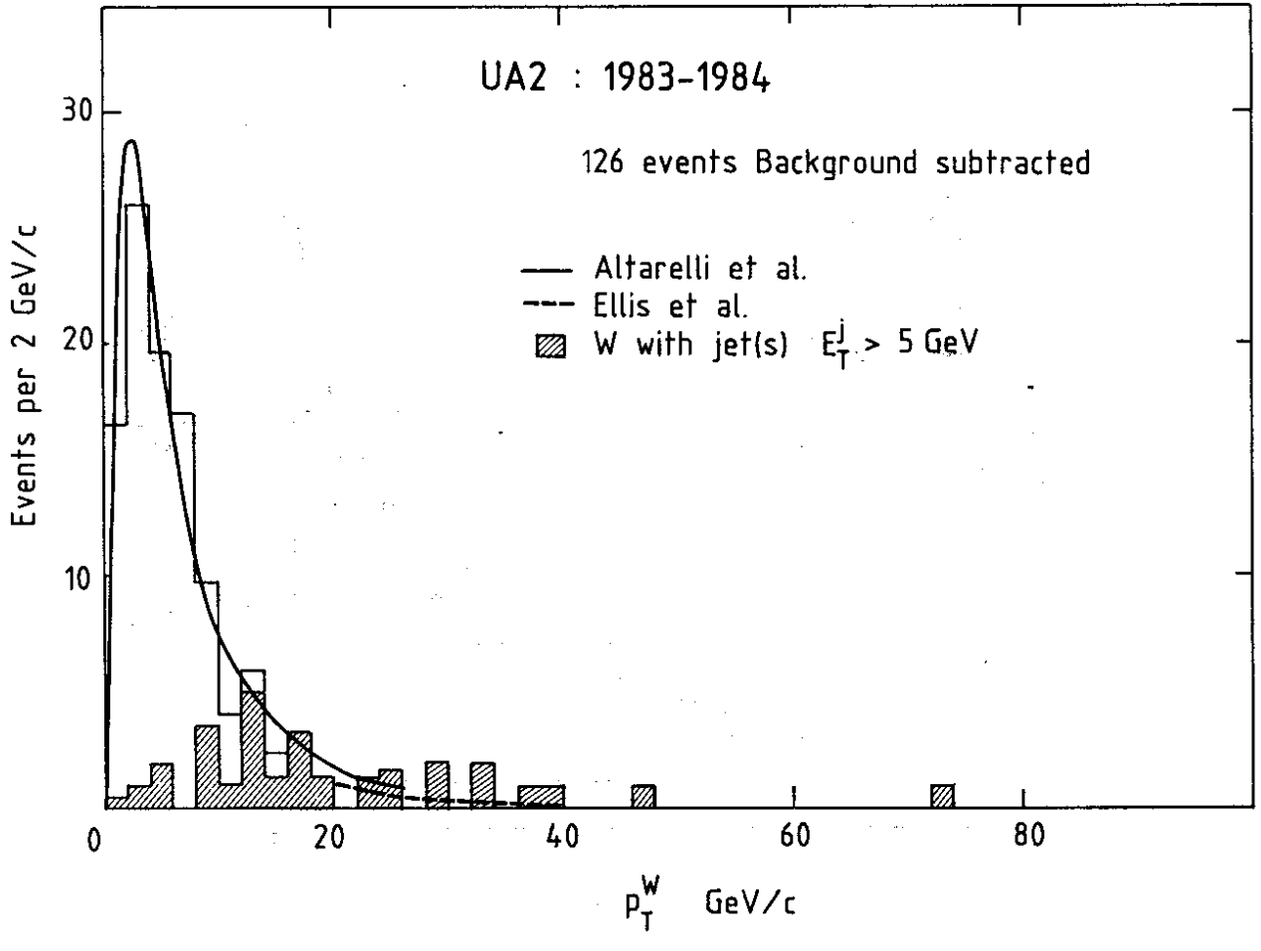
UA2 : 1983-1984
126 events Background subtracted
Altarelli et al.
Ellis et al.
W with jet(s) $E_T^j > 5$ GeV
Events per 2 GeV/c
30
20
10
0
20
40
60
80
p_T^W GeV/c

Fig. 12

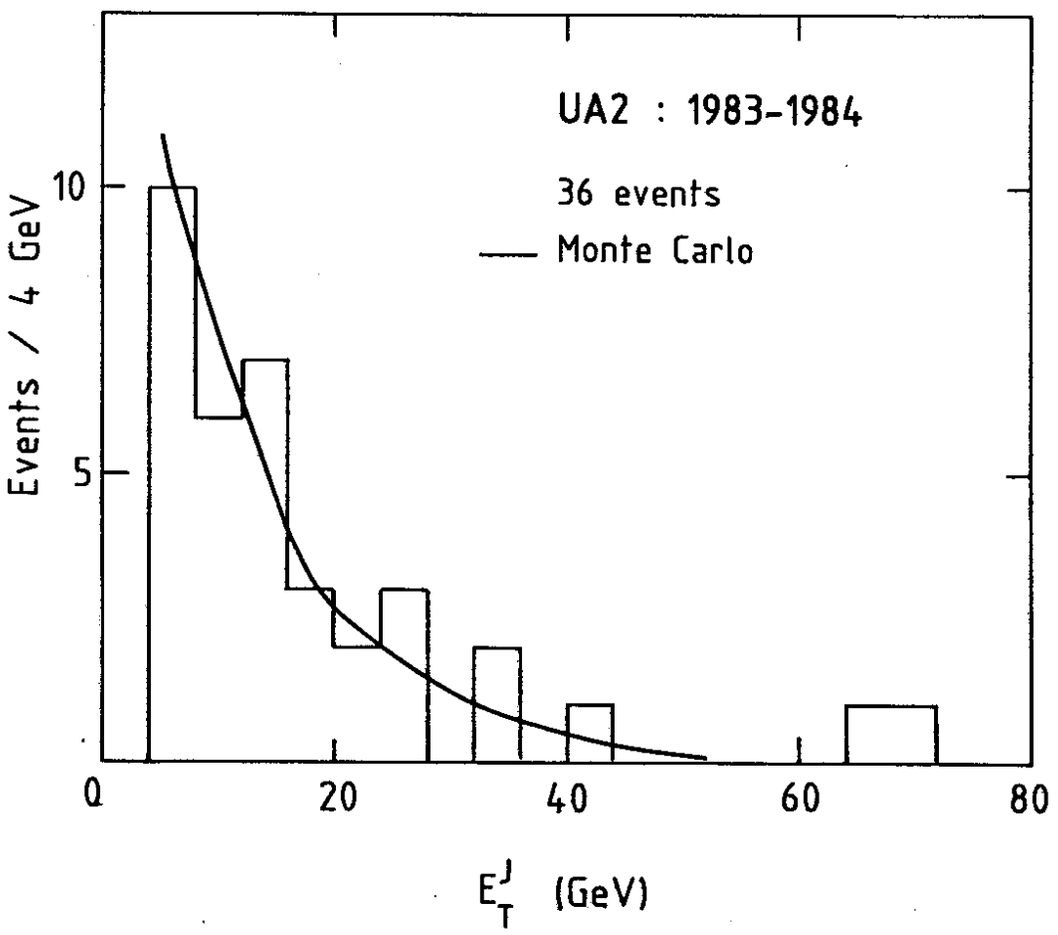
UA2 : 1983-1984
36 events
Monte Carlo
Events / 4 GeV
10
5
0
20
40
60
80
E_T^J (GeV)

Fig. 13

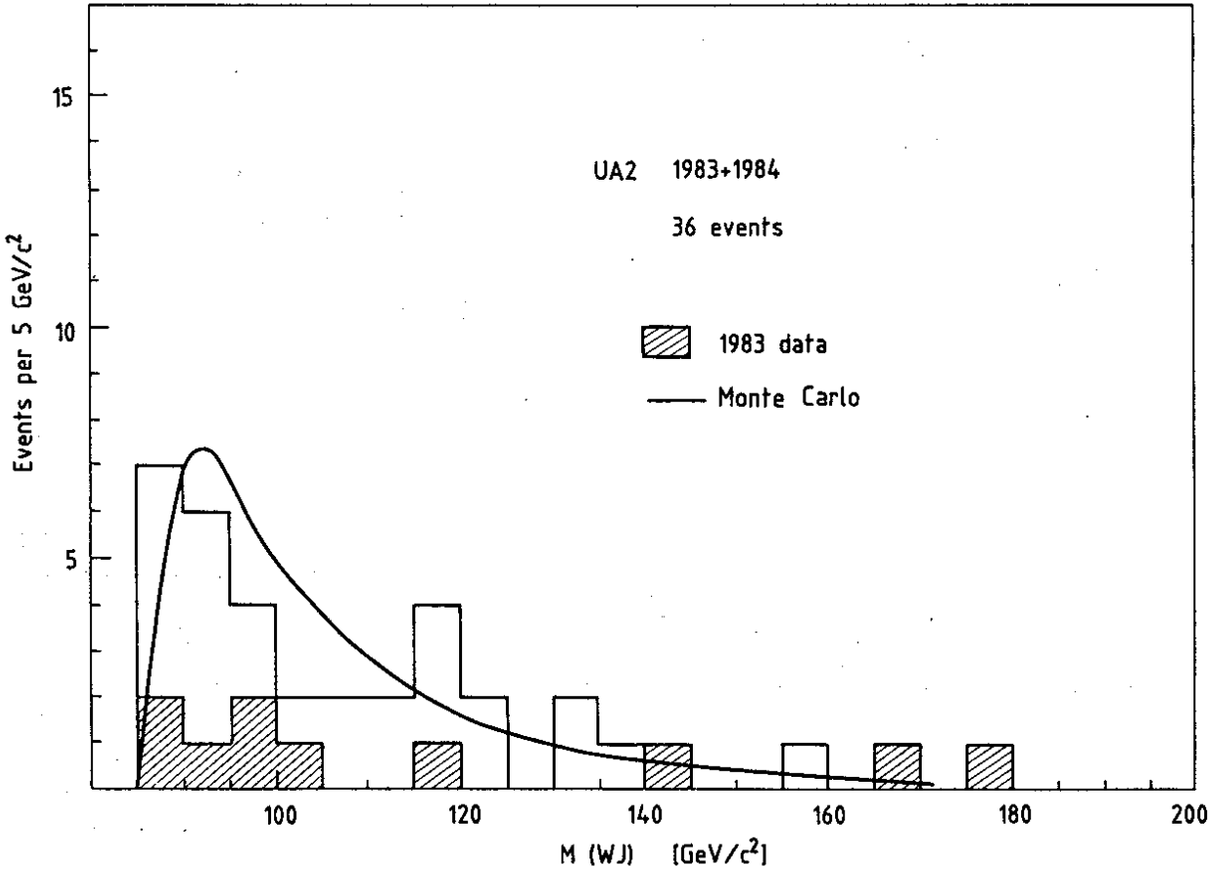
UA2 1983+1984
36 events
1983 data
Monte Carlo
Events per 5 GeV/c²
M (WJ) [GeV/c²]
15
10
5
100
120
140
160
180
200

Fig. 14

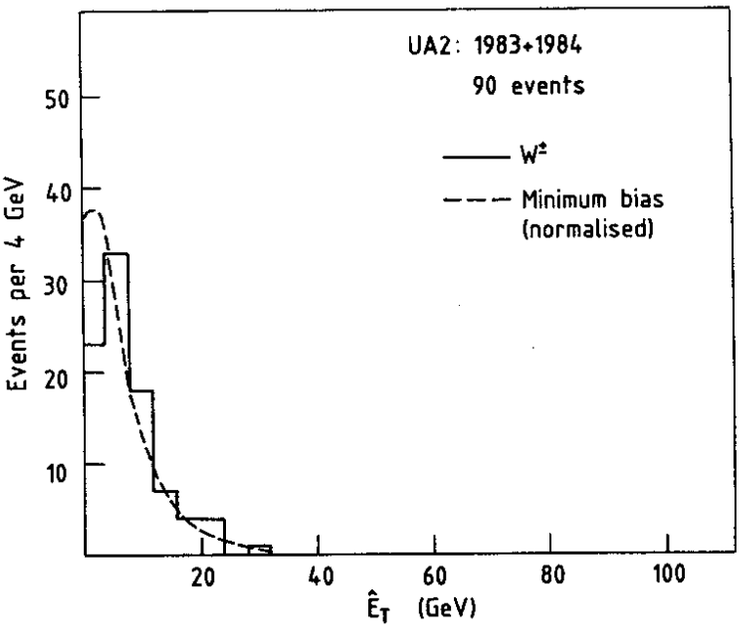
UA2: 1983+1984
90 events
W±
Minimum bias
(normalised)
Events per 4 GeV
50
40
30
20
10
20
40
60
80
100
$\hat{E}_T$ (GeV)

Fig. 15

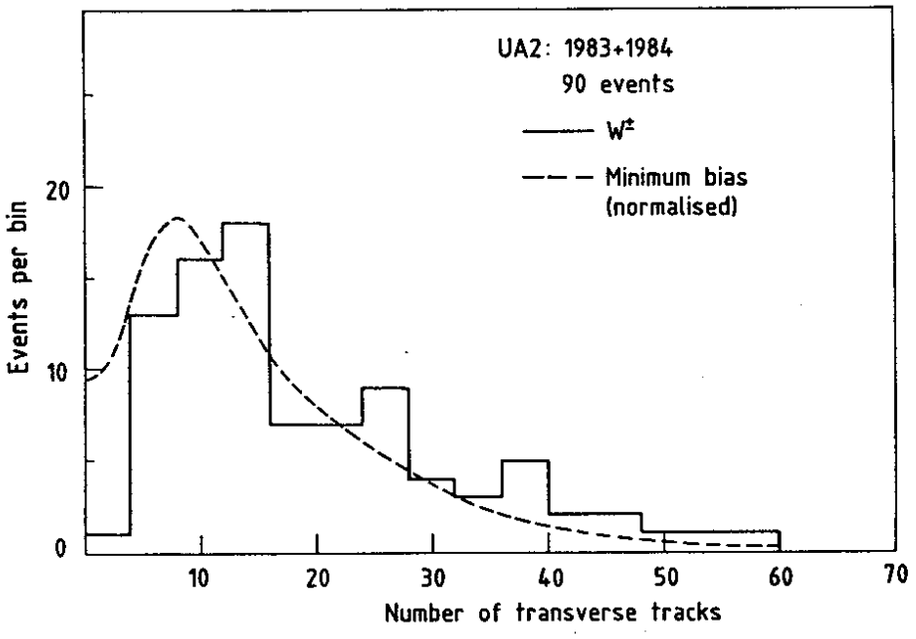
UA2: 1983+1984
90 events
W±
Minimum bias
(normalised)
Events per bin
20
10
0
10
20
30
40
50
60
70
Number of transverse tracks

Fig. 16

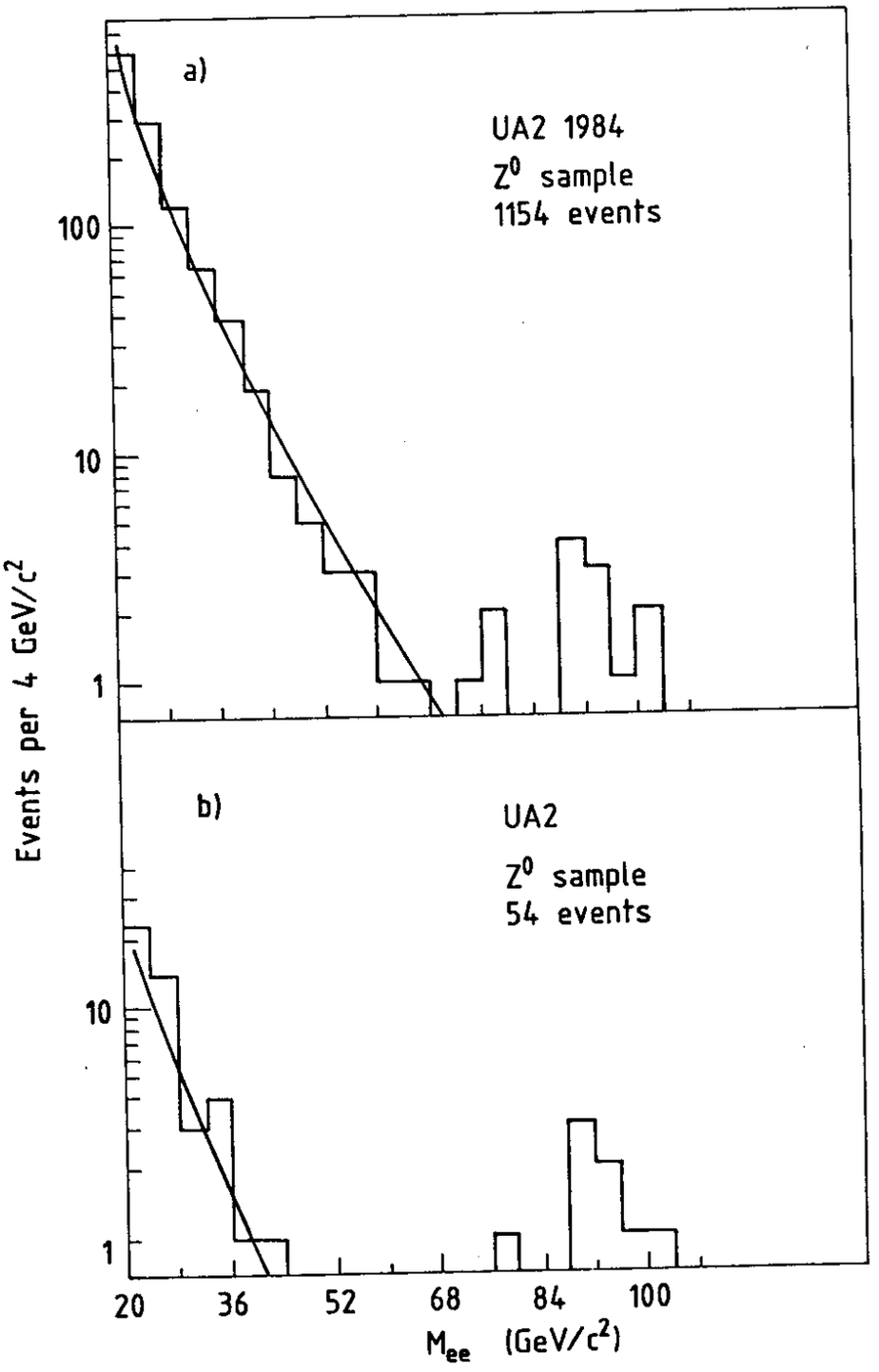
a)
UA2 1984
Z^0 sample
1154 events
100
10
1
b)
UA2
Z^0 sample
54 events
10
1
Events per 4 GeV/c^2
20
36
52
68
84
100
M_{ee} (GeV/c^2)

Fig. 17

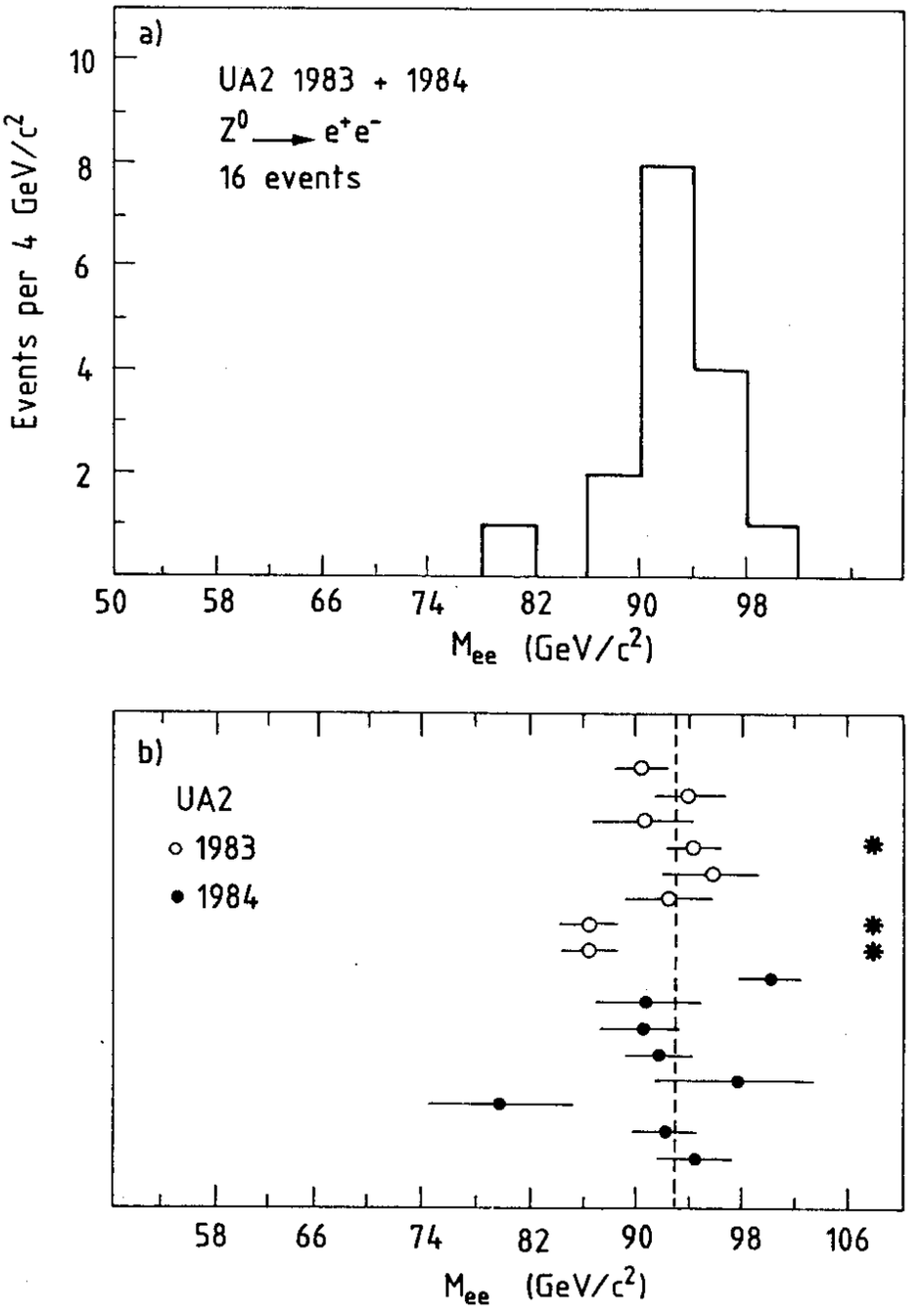
a)
UA2 1983 + 1984
$Z^0 \longrightarrow e^+e^-$
16 events
Events per 4 GeV/c^2
10
8
6
4
2
50
58
66
74
82
90
98
M_{ee} (GeV/c^2)
b)
UA2
○ 1983
● 1984
58
66
74
82
90
98
106
M_{ee} (GeV/c^2)

Fig. 18

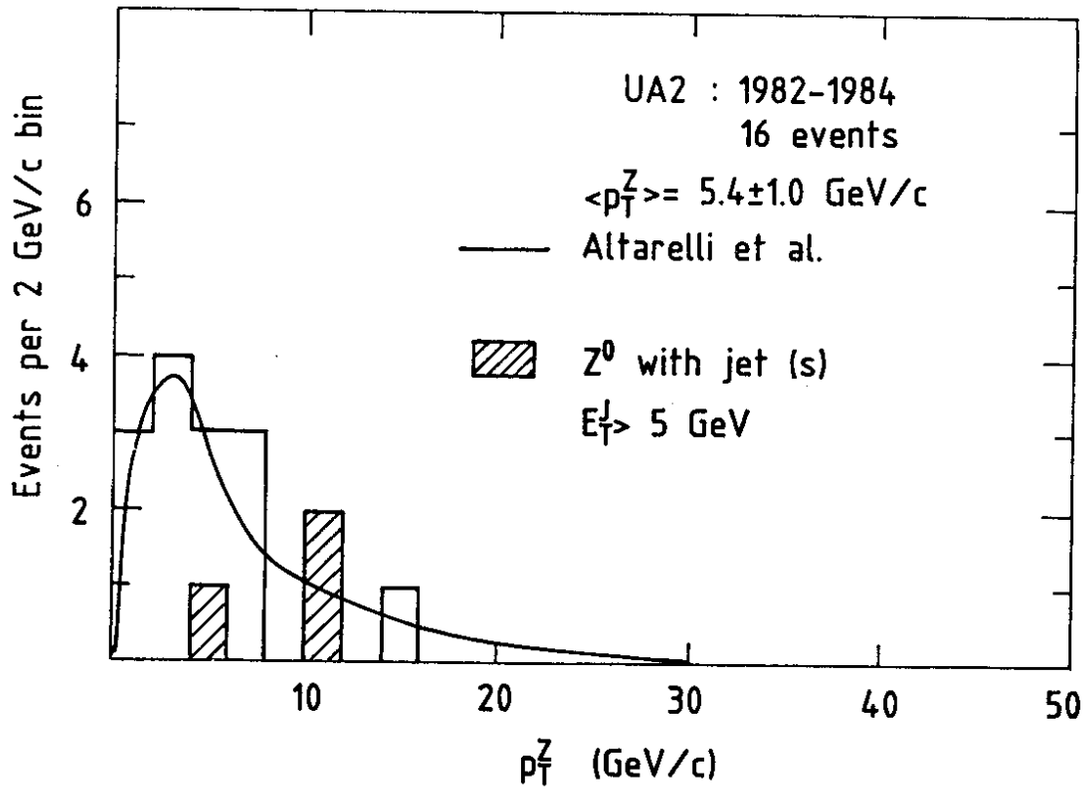
UA2 : 1982-1984
16 events
<p_T^Z>= 5.4±1.0 GeV/c
Altarelli et al.
Z^0 with jet (s)
E_T^J> 5 GeV
Events per 2 GeV/c bin
2
4
6
10
20
30
40
50
p_T^Z (GeV/c)

Fig. 19

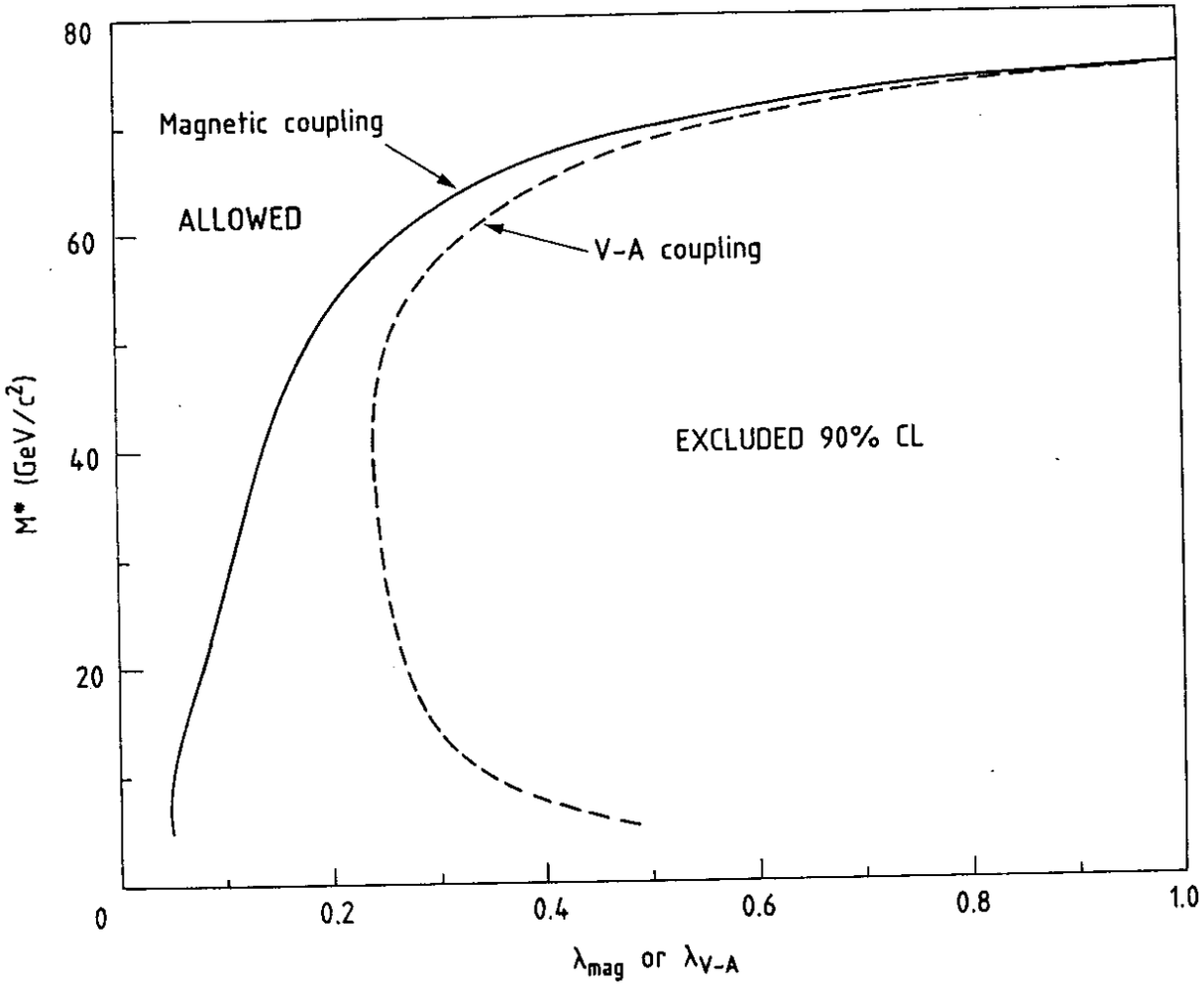
80
60
40
20
0
M* (GeV/c²)
Magnetic coupling
ALLOWED
V-A coupling
EXCLUDED 90% CL
0.2
0.4
0.6
0.8
1.0
λmag or λV-A

Fig. 20

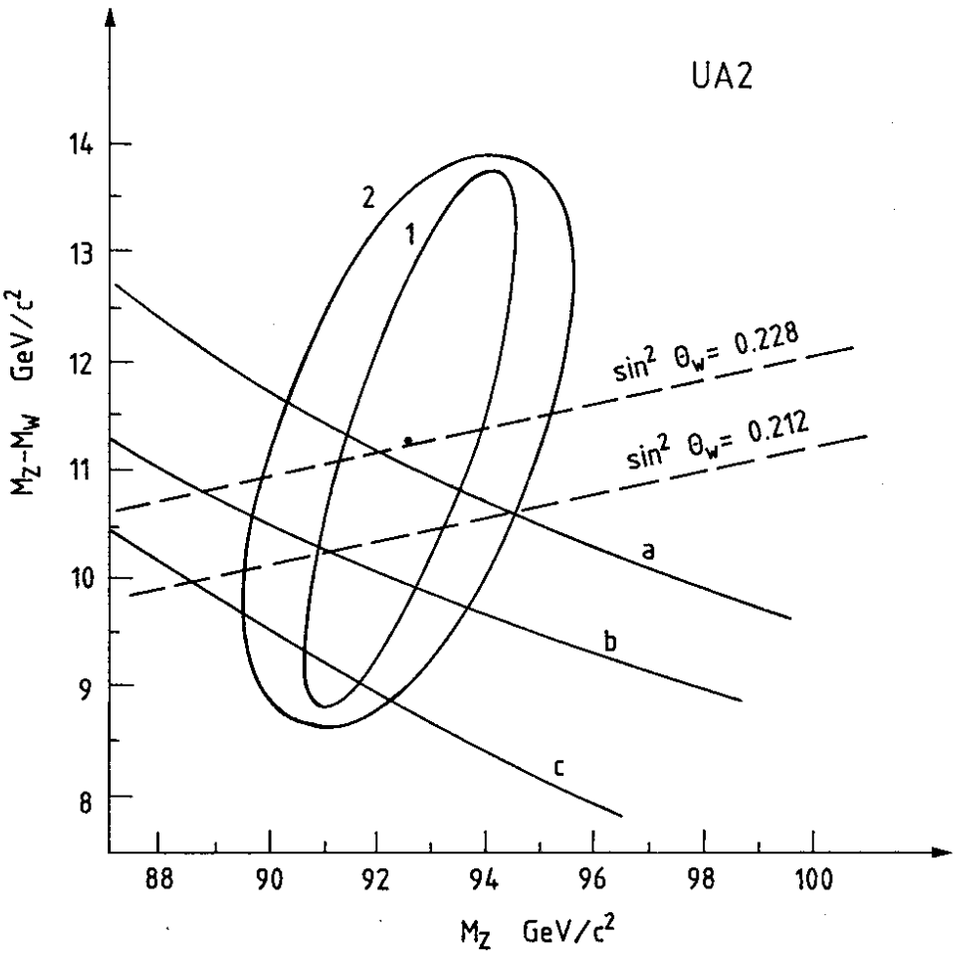
UA2
14
13
12
11
10
9
8
88
90
92
94
96
98
100
$M_Z - M_W$ GeV/c^2
M_Z GeV/c^2
2
1
$\sin^2 \theta_w = 0.228$
$\sin^2 \theta_w = 0.212$
a
b
c

Fig. 21